7-2016

Discovery, Cloning, Expression, Purification, and Characterization of Phosphoglycolate Phosphatase from Staphylococcus aureus

Isreal Moreno
im4514@rit.edu

Discovery, Cloning, Expression, Purification, and Characterization of Phosphoglycolate Phosphatase from *Staphylococcus aureus*

Isreal Moreno

A thesis submitted in partial fulfillment of the requirements for the degree of Master of Science in Chemistry in the School of Chemistry and Materials Science, College of Science Rochester Institute of Technology

July 2016

Signature of the Author_____

Accepted by_____

Director, M.S. Degree Program Date

SCHOOL OF CHEMISTRY AND MATERIALS SCIENCE
COLLEGE OF SCIENCE
ROCHESTER INSTITUTE OF TECHNOLOGY
ROCHESTER, NEW YORK

CERTIFICATE OF APPROVAL

M.S. DEGREE THESIS

The M.S. Degree Thesis of Isreal Moreno has been examined and approved by the thesis committee as satisfactory for the thesis required for the M.S. degree in Chemistry.

Dr. Suzanne O'Handley, *Thesis Advisor*

Dr. Austin Gehret, *Committee Member*

Dr. André O. Hudson, *Committee Member*

Dr. Lea Michel, *Committee Member*

Date

Abstract

Staphylococcus aureus is a major cause of hospital-acquired infections. The multi-drug resistant nature of certain *S. aureus* strains makes the discovery of new drug targets for *S. aureus* vital. A newly discovered virulence factor from *S. aureus* was described as an ortholog of NagD from *E. coli*, a member of the nitrophenyl phosphatase family of the HAD (Haloacid Dehalogenase) superfamily. This thesis will show that this virulence factor is not an ortholog of NagD UMPase from *E. coli*, but rather a phosphoglycolate phosphatase (PGPase). If phosphoglycolate accumulates in the cell, it will inhibit the glycolytic enzyme triose phosphate isomerase (TPI). In *S. aureus*, TPI also serves as an adhesion protein that can bind to host cells; phosphoglycolate would interfere with this adhesion process and thus make it harder for *S. aureus* to infect host cells. Thus, this *S. aureus* PGPase may act as a virulence factor by degrading the TPI inhibitor phosphoglycolate. We cloned the gene, expressed and purified the protein, and determined and characterized its activity. We have subcloned this PGPase into a His•Tag vector, purified the protein using nickel affinity and size exclusion chromatography, and characterized enzymatic activity, optimal conditions (substrate, pH, and metal usage), and kinetics.

Abbreviations

2-PG	2-phosphoglycolate
BCE	Before common era
bp	Base pair
BSA	Bovine serum albumin
C. elegans	*Caenorhabditis elegans*
C. neoformans	*Crytococcus neoformans*
Da	dalton
DHAP	dihydroxy acetone phosphate
DTT	dithiothreitol
E. coli	*Escherichia coli*
EDTA	Ethylenediaminetetraacetic acid
EFI	Enzyme Function Initiative
G3P	glyceralhdyde-3-phosphate
gph	*E. coli* PGPase gene
HAD	Haloacid Dehalogenase
HR	High resolution
HT or His•Tag	Histidine tag
IPTG	Isopropyl-β-D-thiogalactopyranoside
kbp	kilobasepairs
KCl	Potassium chloride
kDa	kilodalton
LB	Luria-Bertani
MES•NaOH	2-(N-morpholino)ethanesulfonic acid with sodium hydroxide
MRSA	Methicillin resistant *Staphylococcus aureus*
MW	Molecular weight
MWCO	Molecular weight cut off
MWMs	Molecular weight markers
NaCl	Sodium chloride
NagD	*E. coli* UMPase
OD	Optical density
PAGE	Polyacrylamide gel electrophoresis
PCR	Polymerase chain reaction
PEG	Polyethylene glycol
PGPase	Phosphoglycolate phosphatase
Pho13	*S. cerevisiae* PGPase
PLPase	Pyridoxal phosphate
pNpp	p-nitrophenyl phosphate
RCF	Relative centralfugal force
RuBisCO	Ribulose-1,5-bisphosphate carboxylase/oxygenase
S. cerevisiae	*Saccharomyces cerevisiae*
S. aureus or (SA)	*Staphylococcus aureus*
SaPGPase	*S. aureus* PGPase
SaPGPase(HT)	*S. aureus* PGPase His•Tagged
SDS	Sodium Dodecyl Sulfate
Supe	supernatant
TE	Tris, EDTA
TED	Tris, EDTA, DTT
Tirs•HCl	Tris(hydroxymethyl)aminomethane Hydrocholride
TP	Time point
TPI	Triose phosphate isomerase
WT	Wild type

Table of Contents

Abstract i

Abbreviations ii

I. Introduction 1

i. History and Importance of Enzymology 1

ii. The Enzyme Function Initiative 1

iii. Haloacid Dehalogenase Superfamily 2

iv. Subfamilies of HAD Superfamily 6

v. The pNppase Subfamily 7

vi. Phosphoglycolate Phosphatases 9

vii. History and Characteristics of *Staphylococcus aureus* 11

viii. Phosphoglycolate Phosphatase in *Staphylococcus aureus* 13

ix. Protein Moonlighting 13

x. Methodology 14

II. Materials and Methods 21

i. Synthetic Gene Design 21

ii. Transformations of pMAT-SaPGPase 21

iii. Plasmid Midiprep 22

iv. Restriction Enzyme Digests 23

v. Ligation 23

vi. Transformation of *E. coli* DH5α with pETSaPGPase and pET19SaPGPase 24

vii. Plasmid miniprep 25

viii. Verification of subcloning 25

ix. Sequencing 26

x. Transformation into BLR (DE3) 26

xi. Overexpression of SaPGPase and SaPGPase(HT) in BLR(DE3) 27

xii. Purification of SaPGPase from BLR(DE3) 28

a. Freeze-Thaw purification 28

b. Size exclusion chromatography 28

xiii. Purification of SaPGPase(HT) in BLR(DE3) 29

a. Cell lysis by sonication 29

b. Ni-NTA His•Tag affinity chromatography 29

b. Bradford assay 31
xv. Enzyme characterization 32
a. Determination of specific activity 32
b. pH optimization 32
c. Metal ion preference 32
d. Metal ion concentration optimization 33
e. Substrate specificity 34
f. Kinetics 35
III. Results and Discussion 36
i. Plasmid Purification 36
ii. Plasmid Digestion and Purification 38
iii. Ligation and Transformation 41
iv. Verification of Subcloning 44
v. Midiprep of pETSaPGPase and pET19SaPGPase 46
vi. Sequencing of pETSaPGPase and pET19SaPGPase 46
vii. Overexpression of SaPGPase(HT) in *E. coli* BLR (DE3) 47
viii. Ni-NTA affinity chromatography of *S. aureus* PGPase(HT) 48
ix. Size exclusion chromatography of *S. aureus* PGPase(HT) 50
x. Overexpression of SaPGPase in *E.coli* BLR(DE3) 52
xi. Ammonium sulfate concentration of SaPGPase 53
xii. Size exclusion chromatography of SaPGPase 54
xiii. Total Purification of SaPGPase(HT) and SaPGPase 56
xiv. Characterization of *S. aureus* phosphoglycolate phosphatase 58
a. Substrate Specificity 59
b. pH optimum 60
c. Divalent metal ion requirements 62
d. Kinetic analysis of *S. aureus* PGPase(HT) and PGPase 64
IV. Conclusions 68
V. References 70
VI. Acknowledgments 74
VII. Appendix 75

I. Introduction

i. History and Importance of Enzymology

Throughout the years, scientists have endeavored to gain insight into how biochemical reactions that would normally take thousands to billions of years, occur in a drastically shorter timescale that allow for life[1]. Enzymes are what give life on Earth this unique ability. The study of enzymes is important in the understanding of life and the advancement of medicine. The commercial use of enzymes by man dates back thousands of years; in fact, the use of enzymes is noted in an ancient Bablyonian text from 2100 BCE[2]. It wasn't until studies in the mid to late 1700's that enzymatic activity would be described by René Antoine Ferchault de Réaumur and Lazzaro Spallanzani, and almost a century later for Wilhelm Friedrich Kühne to coin the term "enzyme" from the Greek word *enzumos*, a term that refers to leavening bread[2].

ii. The Enzyme Function Initiative

In the past two decades, there has been a concerted effort to sequence as many whole genomes of as many organisms as possible (whole genome sequencing projects) as well as determine as many unique protein structures as possible (Structural Genomics Initiative[3]), but what has been lacking is the functional annotation and characterization of all of these proteins. Another problem is that a surprisingly large number of proteins in databases, such as the Protein Data Bank, have been misannotated, meaning they have been assigned functions that they do not actually possess and their real function has still to be elucidated. The Enzyme Function Initiative (EFI) was established to solve this problem. The EFI is a consortium of researchers whose goal is to determine the biologically relevant function of proteins that have not yet been characterized or have been misannotated[4]. The EFI is accomplishing this task by the integration of computational and biological methods, and is separated into Cores and Bridging Projects. The

Cores are: genome searching (to update membership of superfamilies), protein expression (high throughput cloning, expression, and purification of chosen proteins), structural characterization (determination of x-ray crystal structure of purified proteins), computational studies (development and application of computational methods to infer enzymatic activity from protein structure), microbiology studies (to determine *in vivo* function), and data dissemination (to update and maintain the EFI website and database so that the data gathered is readily accessible)[4]. The EFI has five Bridging Projects that are essentially the investigation of five different enzyme superfamilies: amidohydrolase, enolase, glutathione transferase, isoprenoid synthase, and haloacid dehalogenase (more recently also referred to as haloalkanoic acid dehalogenase) superfamilies[4].

iii. Haloacid Dehalogenase Superfamily

The Haloacid Dehalogenase (HAD) superfamily of enzymes is a large group encompassing over 3000 different enzymes with members found in the proteomes of organisms from all three domains of life[5,6]. This superfamily was named for the first enzymes of this superfamily that were characterized, the prokaryotic haloacid dehalogeases[7]. Including the haloacid dehalogenases, there are three other classes of enzymes that compose the HAD superfamily: phosphatases (including ATPases), phosphonatases, and phosphomutases[5,6]. Ninety-nine percent of members that have been uncovered thus far are phosphatases, thus a majority of HAD superfamily members perform the phosphate monoesterase function[6]. The biological roles of these enzymes vary, ranging from secondary metabolism to signal transduction to DNA repair [8]. Figure 1 shows the reactions for each class of enzymes[5]; for each, an aspartate residue is utilized as the nucleophile.

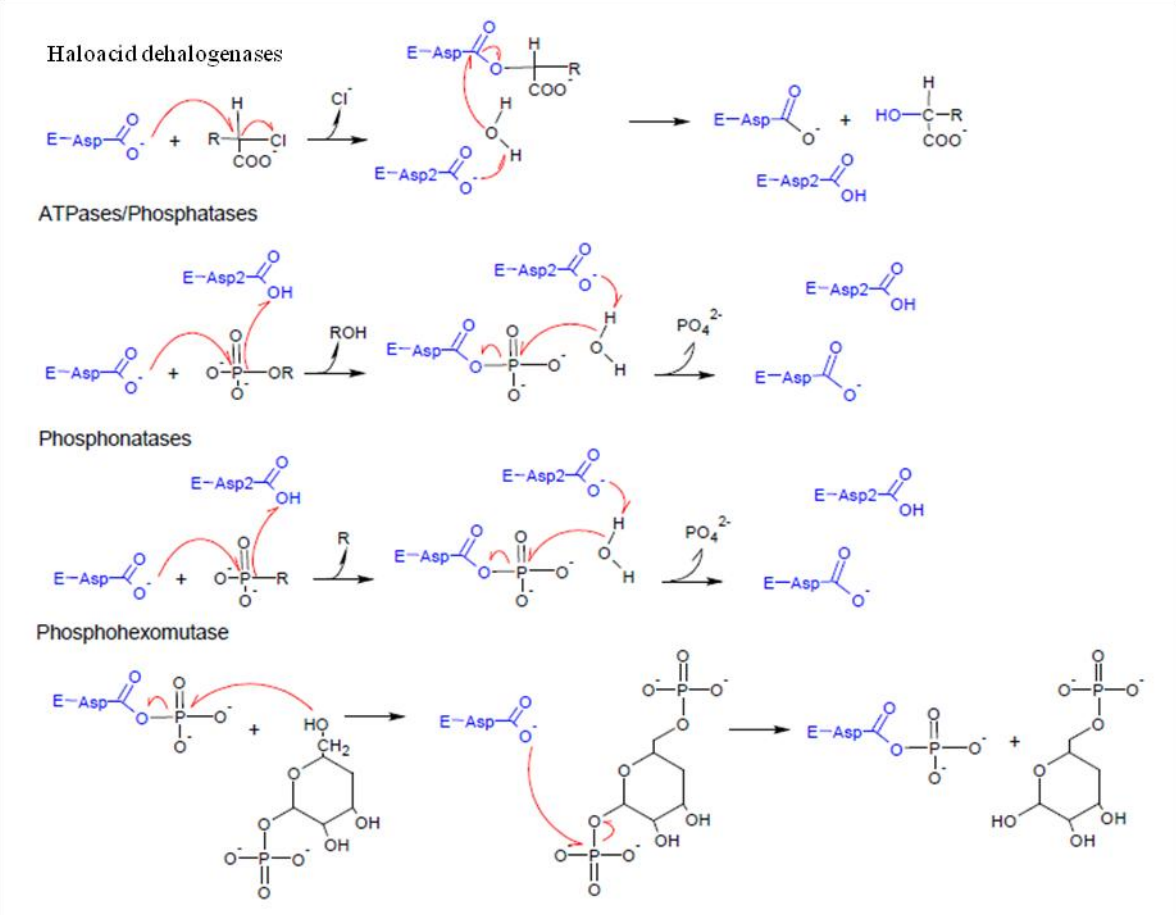

Figure 1: Mechanisms for HAD superfamily members. The four reaction mechanisms above show how the members of the HAD superfamily utilize a catalytic aspartic acid for catalysis.

The basic structure of the core domain of all HAD superfamily members is the same (shown in Figure 2)[5,6,8]. This core domain consists of a three layered α/β sandwich that is composed of repeating β-α units, characterized as the Rossmann fold[5,6,8]. Two structural features differentiate the Rossmann fold in the HAD superfamily from other types of Rossman folds: the "squiggle" and "flap" elements defined by Burroughs et al[5]. The "squiggle" is comprised of six residues that almost create a single helical turn. The "flap" is downstream of the "squiggle" and is a β-hairpin turn projecting out of the core domain[5,6].

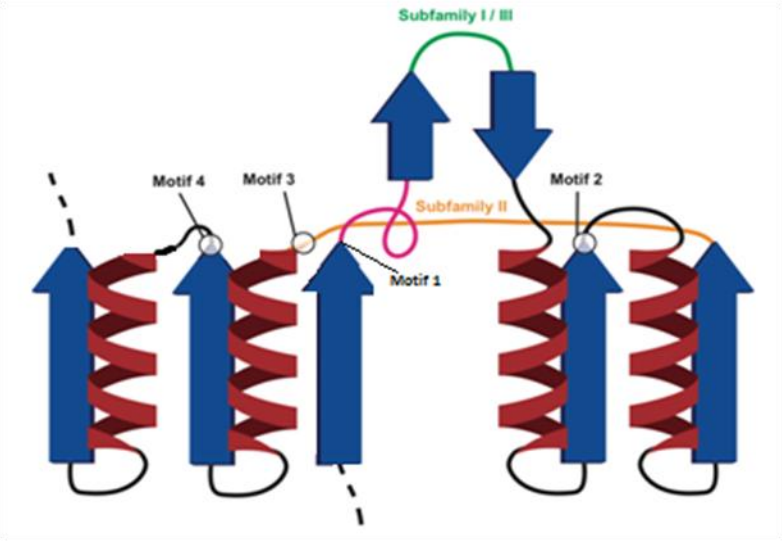

Figure 2: General HAD structure. Shown is the general structure found in members of the HAD superfamily. The characteristic Rossmann fold is shown along with the squiggle (pink) and flap (green) elements. The position of the four conserved motifs and cap domain insertion sites are also shown.

Sequence alignments of HAD superfamily members show ~15% similarity overall and reveal the conservation of four motifs that contain key catalytic amino acids[6]. Note here that the term "motif" as coined by Koonin and Tatusov refers to the conserved amino acid sequences among HAD superfamily members and differs from the more standard definition of "motif" in protein structures[7]. Motif 1 contains the sequence DxD, which is two aspartic acid residues separated by any amino acid[5,6,8]. The carboxylate groups of both of the aspartates coordinate to a divalent metal ion (M^{2+}) cofactor as well as playing other key roles in catalysis[8]. All phosphotransferases within the superfamily possess maximal activity with Mg^{2+}; however, Zn^{2+}, Co^{2+}, and Mn^{2+} can also be utilized[9]. The divalent metal ion cofactor shields the negative charge of the nucleophilic aspartate side chains and stabilizes the phosphoryl group of the substrate (see Figure 3)[10]. A serine or threonine residue within motif 2 and a lysine residue within motif 3 serve to stabilize the reaction intermediates of the hydrolysis reaction[5,6,8]. Motif 4 can be one of three sequences depending on the HAD superfamily enzyme in question: DD, GDxxxD or GDxxxxD[5]. These

aspartate or glutamate residues also serve to coordinate the M^{2+} cofactor with motif 1. The amino acids within these four motifs are found in the active site (Figure 3) and it is one of the aspartates within motif 1 that is responsible for the dephosphorylation reaction. The first aspartate nucleophilically attacks the phosphate group, allowing the –OR group of the substrate to leave, usually resulting in the formation of a hydroxyl group[10,11]. The second aspartate residue deprotonates a nearby water molecule and the resulting hydroxide ion attacks the phosphoaspartyl enzyme intermediate causing the first aspartate to act as a leaving group thus generating free phosphate[11]. The nucleophilic aspartate is beneficial as aspartate can act as a good leaving group as well as a good nucleophile[11].

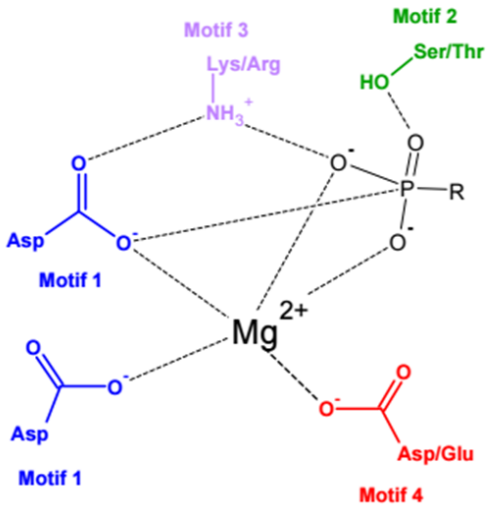

Figure 3: Schematic of HAD family active sites. The schematic shows the location of the four conserved motifs and how each coordinates with either the divalent metal ion cofactor or substrate.

iv. Subfamilies of HAD Superfamily

The HAD superfamily is separated into three subclasses based on the presence of insertions called cap domains that are in addition to the catalytic core domain (see Figure 2)[5,6,8]. Subfamily I cap domains contain an α-helical-bundle domain inserted into the flap element indicated by the green line in Figure 2. This bundle varies in complexity among specific enzymes and ranges from a basic bi-helical α-hairpin to globular multi-helical bundles[5]. This insertion would "close" over the active site upon substrate binding and "open" to allow the leaving group to exit; for this reason, subfamily I members act predominantly on small substrates[6]. Subfamily I consists of haloacid dehalogenases, phosphonatases, and phosphomutases[5,6]. Subfamily II contains a cap domain that is typically composed of α/β sandwiches with a core β-sheet. This insertion site is indicated in Figure 2 as an orange line. This cap domain is not mobile like the subfamily I cap domain; instead, the insertion forms a cavernous structure that is sealed off by movement of the "squiggle-flap" motif only, thus subfamily II members also act upon small substrates[5]. All of the enzymes in subfamily II are phosphatases. The final class, subfamily III, contains no large insertion, thus no cap, leaving the active site exposed on one side to the solvent[5,8]. For this reason, subfamily III enzymes typically catalyze reactions with larger substrates; enzymes in this subfamily are protein phosphatases[5].

Subfamily II can be further broken down as NagD-like proteins (subfamily IIa) and Cof-like proteins (subfamily IIb)[5]. They are classified together due to the fact that they have the same insertion site for their cap domain. The distinguishing characteristic between subfamily IIa and subfamily IIb is the arrangement of the β sheets of the cap domain. Subfamily IIa members have four parallel β-sheet strands whereas subfamily IIb members have three anti-parallel β-sheet strands[5]. A majority of HAD phosphatases are within subfamily IIb; fewer enzymes fall into

subfamily IIa. All members of subfamily IIa are capable of hydrolyzing a phosphate from para-nitrophenyl phosphate, hence the name, the p-nitrophenyl phosphatase (pNppase) subfamily of the HAD superfamily.

v. The pNppase Subfamily

The HAD superfamily was identified by Koonin et al. through the computer analysis of bacterial haloacid dehalogenases using an iterative approach to search sequence databases[7]. This approach utilized BLAST searches, alignments, and other bioinformatic tools with the goal of delineating a superfamily and potential subfamilies. One subfamily that was identified through cluster analysis based on BLAST scores was the pNppase subfamily (see Figure 4)[7]. At that time the only enzymes of this subfamily that had been characterized were two orthologs from two different yeasts, *Saccharomyces cerevisiae* and *Schizosaccharomyces pombe,* and even the natural substrates for those enzymes were not known; activity had only been found for the non-natural substrate pNpp. The first member of the subfamily to be identified with activity on a natural substrate was YZGD. YZGD from *Paenibacillus thiaminolyticus* is a pyridoxal phosphatase (PLPase) with a second domain that belongs to the NUDIX hydrolase superfamily[12]. A human PLPase, without a NUDIX domain, has also been characterized and is believed to play a role in vitamin B_6 metabolism in erythrocytes[13]. NagD from *E. coli* is a UMPase and it is hypothesized to be involved in the regulation of cell wall and polysaccharide biosynthesis[12] as well as pyrimidine homeostasis[14]**.** NagD is the first enzyme of the pNppase subfamily for which the structure has been determined[8]. AraL from *Bacillus subtilus* has been identified as a sugar phosphatase[15]. Of particular interest to us are the phosphoglycolate phosphatase (PGPase) members of the subfamily, which is the topic of the next section.

Figure 4: Sequence alignment of pNppase family members. The amino acid sequences of phosphoglycolate phosphatase from *S. aureus*, *S. cerevisiae* (Pho13), *S. pombe*, and *C. rinhardtii* (PGP2), NAGD from *E. coli*, AraL from *B. subtilits*, pyridoxial phosphatase (PLPase) from humans, and YZGD from *P. thiaminolyticus* were aligned using CLUSTALX. Similar and identical amino acids are in boldface, with identical amino acids indicated with '*'. Gaps in the amino acid sequences are inserted to optimize alingments (indicated by '-'). Motifs I, II, II, and IV of the HAD superfamily are underlined and labeled.

vi. Phosphoglycolate Phosphatases

Phosphoglycolate phosphatase (PGPase) is responsible for the cleavage of phosphate from 2-phosphoglycolate (2-PG) (Figure 5**)**. In photosynthetic organisms, 2-phosphoglycolate is generated by Rubisco (ribulose-1,5-bisphosphate carboxylase / oxygenase)[16,17]. In carbon dioxide-rich environments, Rubisco catalyzes the reaction of carbon dioxide with ribulose-1,5-bisphosphate to generate 2 molecules of 3-phosphoglycerate[18]. 3-phosphoglycerate is converted to glyceraldehyde 3-phosphate (G3P)[18], an intermediate of glycolysis.

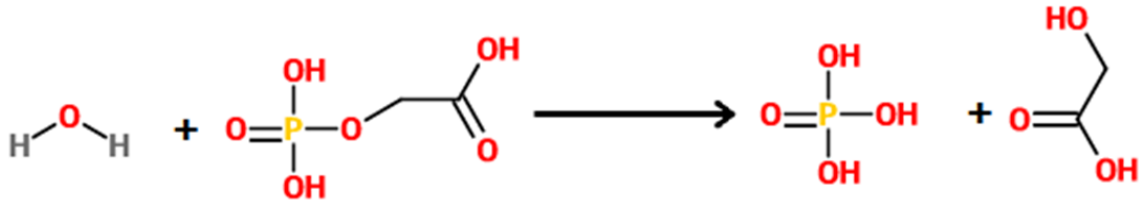

Figure 5: Chemical reaction of phosphoglycolate phosphatase activity. Shown is the hydrolysis of 2-phosphoglycolate releasing phosphate and glycolate. Figure was made using ChemSketch.

Rubisco is also capable of utilizing molecular oxygen to react with ribulose-1,5-bisphosphate, a process known as photorespiration[18]. The reaction between oxygen and ribulose-1,5-bisphosphate generates one molecule of 3-phosphoglycerate and one molecule of 2-phosphoglycolate. The 3-phosphoglycerate enters glycolysis, but 2-phosphoglycolate appears to be a dead-end metabolite and thus must be degraded by PGPase. The resulting glycolate can be converted to glycine, which is utilized by the cell[18]. Studies have shown that PGPase-deficient strains of *Arabidopsis thaliana*, *Hordeum vulgare* (barley), and *Chlamydomonas reinhardtii* (algae) can only grow under high CO_2 conditions[16]. This indicates that an accumulation of 2-phosphoglycolate is detrimental to the cell. One reason that this accumulation could be harmful is that 2-phosphoglycolate is a strong inhibitor of triose phosphate isomerase (TPI), an important

glycolytic enzyme; 2-phosphoglycolate acts as a transition state analog and binds 100 times more tightly to TPI than do its substrates[19,20]. The crystal structure of 2-phosphoglycolate bound to the active site of TPI has been solved to a resolution of 2.5 Å[19]. Rubisco utilizes CO_2 and O_2 in a 4:1 ratio in normal atmospheric conditions so PGPase must be expressed to ensure phosphoglycolate does not inhibit TPI, blocking glycolysis or gluconeogenesis[18].

The only confirmed way of producing phosphoglycolate *in vivo* is in the above photorespiratory pathway, but the presence of PGPase in non-photosynthetic organisms indicates 2-phosphoglycolate must be produced by a non-photosynthetic means as well. Exactly how 2-phosphoglycolate is produced in non-photosynthetic organisms has yet to be established. Of the PGPases from non-photosynthetic organisms, a few have been studied in depth.

The PGPase from *S. cerevisiae*, Pho13, may play a role in xylose metabolism as *S. cerevisiae* that lack Pho13 are more fit for growth with a xylose carbon source[21–23]. Xylose is not a natural carbon source for *S. cerevisiae*, however engineered strains that include key enzymes such as xylose reductase and xylitol dehydrogenase can metabolize xylose to ethanol (a key process in the development and production of biofuels since xylose composes ~40% of cellulosic biomass[24]).

In *E. coli*, the *gph* gene encodes a PGPase that appears to be involved in DNA repair[17]. In the repair process, 3'-phosphoglycolate ends that are generated by oxidative damage to DNA are repaired to generate free 2-phosphoglycolate[17]. When *E. coli* was treated with bleomycin (an agent that oxidatively damages DNA) levels of 2-phosphoglycolate were significantly increased in *gph* mutants, as compared to wild type *E. coli*[17].

In erythrocytes, 2-phosphoglycolate is a potent effector of the bisphosphoglycerate shunt (a major modifier of the oxygen affinity of hemoglobin)[25]. 2-phosphoglycolate may be produced by the phosphorylation of glycolate via pyruvate kinase[26].

vii. History and Characteristics of *Staphylococcus aureus*

S. aureus is a gram-positive bacterium and a facultative anaerobe; the bacteria is capable of growing in aerobic and anaerobic conditions, switching between aerobic respiration and fermentation[27]. Prior to 1880, the cause of infection after surgery was not precisely known. When Swedish surgeon Alexander Ogston inoculated chicken eggs with pus from patients, he observed clusters of circular bacteria growing in the eggs[28]. To prove that this bacterium was the actual cause of infection, he inoculated guinea pigs and mice with pus taken from patients. These animals developed similar symptoms, abscesses, and diseases as the patients. He named this new bacterium *Staphylococcus* (*staphyle* meaning "bunch of grapes" and *kokkos* meaning berry), based on its appearance under a microscope[28,29]. Four years later, when the German surgeon Anton Rosenbach grew this new bacterium on media, he discovered two different strains through different pigmentation of the colonies. He named the one that had a golden appearance *S. aureus* and the white form *S. albus* (later renamed *S. epidermis*), and thus, Rosenbach is often credited as the discoverer of *S. aureus*[28].

The main habitat of *S. aureus* is the nose and skin of warm-blooded animals[27]. It is a persistent resident on 20%, and found intermittently on ~60%, of the human population[30].This bacterium produces toxins and super-antigens that cause a wide range of diseases including toxic shock syndrome, scarlet fever, scalded skin syndrome, endocarditis, necrotizing pneumonia, food-borne illnesses, skin infections, and sepsis[27,31–33]. In 2011, the CDC reported ~80,000 life-threatening *S. aureus* infections in the United States [33]. In fact, more people die in the United

States from these infections than from HIV/AIDS each year[34]. *S. aureus* is especially challenging to treat for two reasons: 1) it is capable of causing widespread infections by "hiding" from the immune system through its multiple and redundant virulence factors and 2) its increasing antibiotic resistance[27,35,36].

S. aureus is a highly promiscuous organism capable of acquiring resistance and virulence genes from other bacterial species through horizontal gene transfer. Antibiotic resistance can also arise through mutations that alter the structure of an antibiotic target[27,30,35,36]. Almost as soon as the β-lactam antibiotic penicillin was introduced, strains of penicillin-resistant *S. aureus* arose[31,36]. To fight those infections, methicillin (a derivative of penicillin) was introduced, but again resistance arose. Methicillin-resistant *Staphylococcus aureus* (MRSA) acquired a mutation in the penicillin-binding protein MecA that was no longer able to bind to β-lactam drugs[27,36,37]. Originally, MRSA was only contracted within a hospital setting and was thus called hospital-associated MRSA; however, as early as 1990, MRSA was found in patients who had not been to a hospital nor in contact with anyone who had been, and consequently community-associated MRSA emerged[31,36]. At that time the "antibiotic of last resort", vancomycin, was the only remaining antibiotic that could reliably be used to treat MRSA infections[38]. Subsequently, strains of *S. aureus* acquired vancomycin resistance from enterococci bacteria, and depending on the exact genes acquired, became either less sensitive to or fully resistant to vancomycin[27,36]. In addition, there are other strains of MRSA that are on the rise such as epidemic MRSA and livestock-associated MRSA[35]. Therefore, there is a great need to discover novel antibiotic targets to treat infections of these super resistant strains of *S. aureus*, as well as other multidrug-resistant pathogenic bacteria. These targets could be proteins essential to the survival of the pathogen or virulence factors that allow the pathogen to cause disease.

viii. Phosphoglycolate Phosphatase in *Staphylococcus aureus*

A study by Begun et al. to identify novel *S. aureus* virulence factors uncovered several key virulence factors, including a pNppase family member[39]. In this study, they used a *Caenorhabditis elegans* killing model, which highly correlates virulence factors that kill *C. elegans* to those involved in pathogenesis of vertebrate models[39]. Through screening 2,950 *S. aureus* mutants, they identified 145 mutants that had attenuated virulence. Most of these virulence factors had already been identified, but five were not previously known[39]. These five mutants with attenuated virulence were next studied in a murine renal abscess model in which only one, SAV0929 which they identified as NagD, showed a significant decrease in virulence[39]. Begun et al. misannotated SAV0929 as NagD nucleoside monophosphatase based simply on sequence similarity; however, we show, in this thesis, that SAV0929 is instead a PGPase.

ix. Protein Moonlighting

The hypothesized role of this PGPase virulence factor may be explained by enzymatic moonlighting. Many enzymes that were originally thought to be simply housekeeping enzymes, such as those found in glycolysis, have been shown to perform unexpected secondary functions, a concept referred to as moonlighting[40,41]. It is incongruous that a glycolytic enzyme, which is found in nearly every organism, would increase virulence of a pathogen, but many of these enzymes have been proven to be important virulence factors for pathogenic bacteria[40,41]. An example of a glycolytic enzyme that has surprising moonlighting characteristics is triose phosphate isomerase (TPI) from *S. aureus*[40,42]. Studies by Pancholi et al.[43] and Ikeda et al.[42,44] have shown that TPI from *S. aureus* is capable of binding to glucuronoxylomannan, the main component of the capsule of *Crytococcus neoformans*, a microbe that *S. aureus* infects[42]. This interaction was further investigated through the use of docking simulation experiments. The

interaction between TPI and the capsule of *C. neoformans* would only be plausible if TPI was expressed on the cell surface of *S. aureus*. Yamaguchi et al. used scanning immunoelectron microscopy to confirm the presence of TPI on the cell surface of *S. aureus*[45]. Triose phosphate isomerase's moonlighting ability, as a cell surface protein, allows it to act as a virulence factor through host cell adhesion.

Since phosphoglycolate is an inhibitor of TPI[19,20], we hypothesize that phosphoglycolate could reduce TPI's adhesion to host cells thus reducing virulence, and that PGPase could act as a virulence factor by degrading and removing phosphoglycolate, allowing TPI to act as an adhesion virulence factor. Since Begun et al. showed SAV0929 to be a virulence factor for *S. aureus*, it is crucial to characterize this enzyme to help defeat the spread of *S. aureus*, including antibiotic resistance strains. The characterization of this enzyme as a phosphoglycolate phosphatase is described in this thesis.

x. Methodology

Our research group is interested in characterizing the SAV0929 from *S. aureus*. When a previous member of our lab cloned the gene, two mutations, I132V and Y209C, were introduced during PCR (polymerase chain reaction) amplification of the gene from genomic DNA (ATCC). Rather than risk introducing mutations again via PCR, we could have chosen to either perform site-directed mutagenesis or design a synthetic gene. Because there were two mutations to correct, we decided to design a synthetic gene (Figure 6).

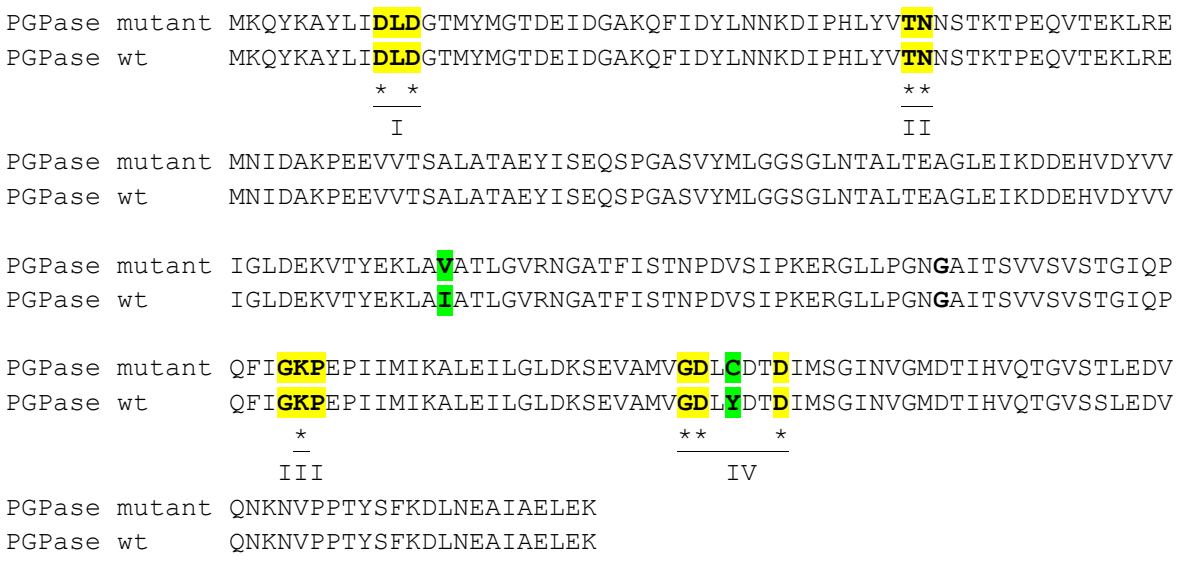

Figure 6: Sequence alignment of Wild-Type and mutated PGPase from *S. aureus*. The sequence alignment comparing the normal (wild-type) protein sequence for the phosphoglycolate phosphatase (PGPase) from *S. aureus* and the protein sequence of the enzyme that had previously been characterized in the lab. The HAD motifs are highlighted in yellow while the two mutations are noted in green. The mutations are I132V and Y209C.

A synthetic gene was designed that matched the sequence of SAV0929 (gene encoding the PGPase) from *S. aureus* Mu50. Restriction sites for XbaI and NdeI were added to the 5' end of the gene and restriction sites for BamHI-HF and HindIII were added to the 3' end of the gene, for subcloning. SAV0929 contains a NdeI site and a HindIII site, thus two silent mutations were introduced to remove these sites without changing the encoded amino acids (Figure 7). This synthetic gene was delivered in the plasmid pMAT-SaPGPase.

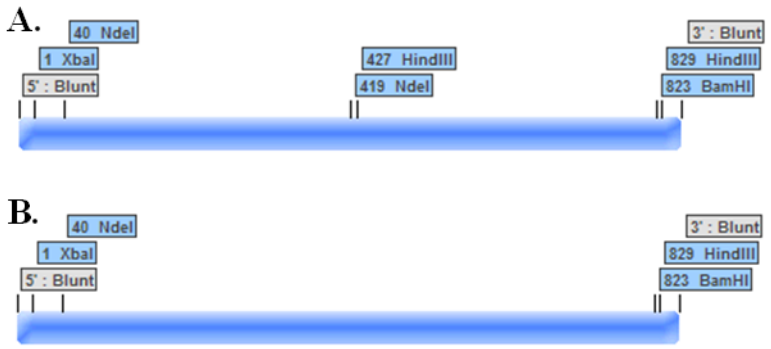

Figure 7. Predicted restriction sites for wildtype gene and synthetic gene. (a. wild type b. synthetic gene) Restriction sites are shown for BamHI, HindIII, NdeI, and XbaI enzymes.

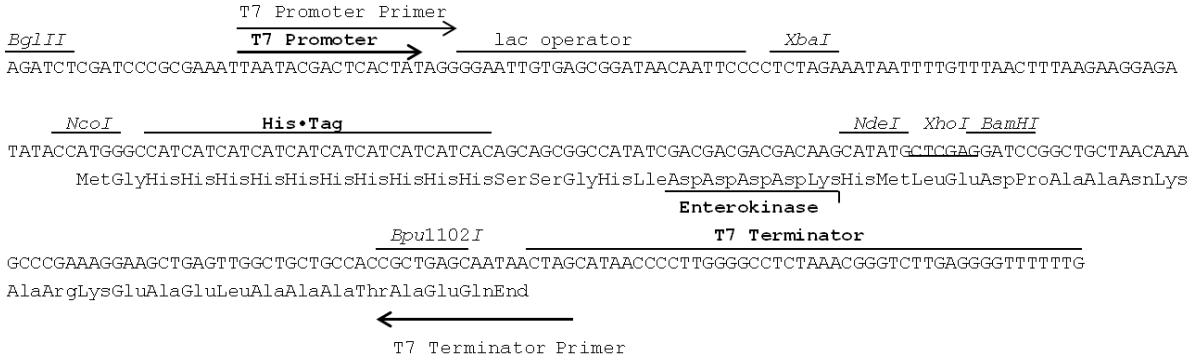

Figure 8. pET19b cloning and expression region. The region of the pET19b vector containing the T7 promoter and terminator sequence, lac operator, His Tag, and various restriction sites.

This synthetic gene was subcloned into pET11b and pET19b plasmids. Both of these expression systems include a T7 *lac* promoter/operator for overexpression (see Figure 8)[46]. The *lac* operator is downstream of the promoter and allows for the binding of the lac repressor, inhibiting transcription by preventing T7 RNA polymerase from binding, thus reducing basal expression. An *E. coli* lac promoter controls transcription of the T7 RNA polymerase gene that is encoded in (DE3) strains of *E. coli*. Lac promoters can be induced by the addition of isopropyl β-D-thiogalactopyranosidase (IPTG)[46]. The structure of IPTG is similar to allolactose, a natural

inducer for the lac promoter. IPTG binds to the lac repressor, allowing the T7 RNA polymerase gene to commence transcription. pET19b also contains a sequence 5' to the NdeI restriction site that codes for a string of 10 histidines to create a His•Tag on the N-terminal end of the protein[46]. Figure 9 shows schematics of pET11b, pET19b, and pMAT-SaPGPase while Figure 10 shows the process of subcloning.

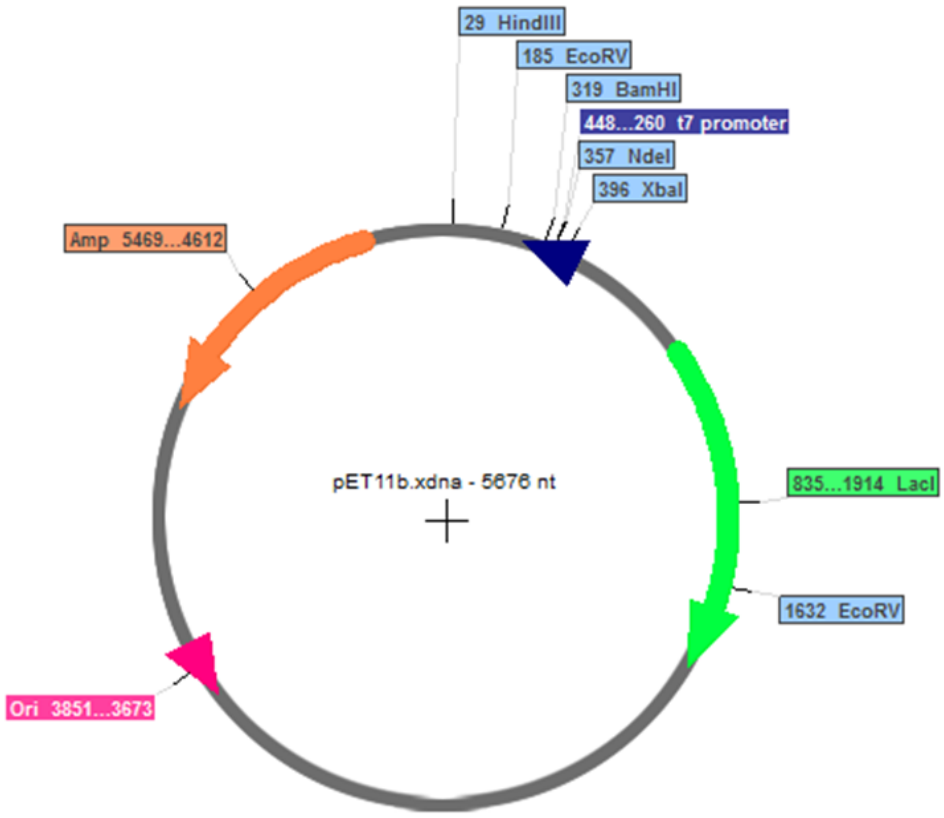

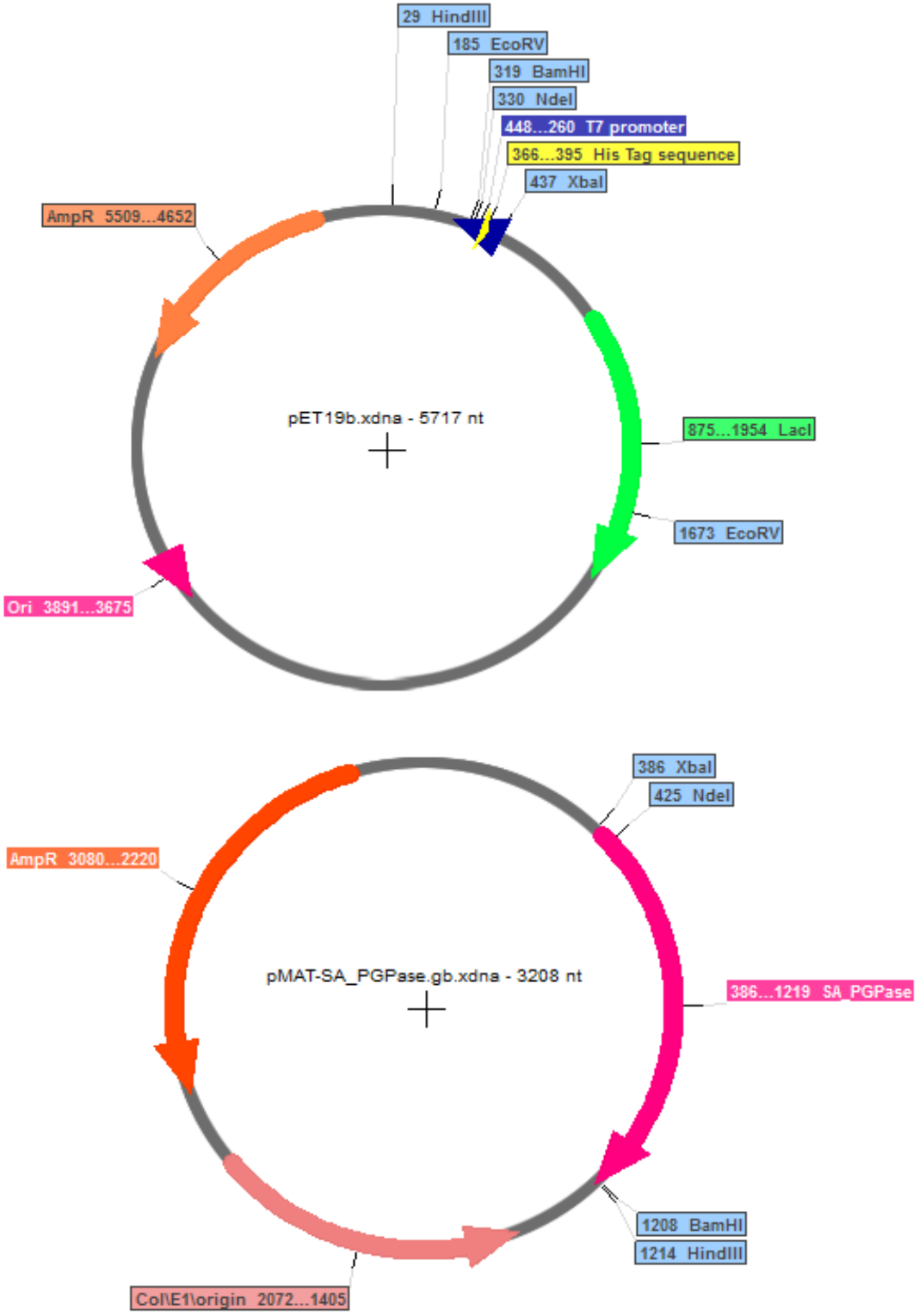

Figure 9: Plasmid maps of pET11b, pET19b, and pMAT-SaPGPase. pET11b containing a T7 *lac* promoter. pET19b containing a T7 *lac* promoter and a His•Tag coding sequence. pMAT-SaPGPase containing SAV0929. EcoRV, NdeI, XbaI, HindII, and BamHI restriction sites are shown for all plasmids.

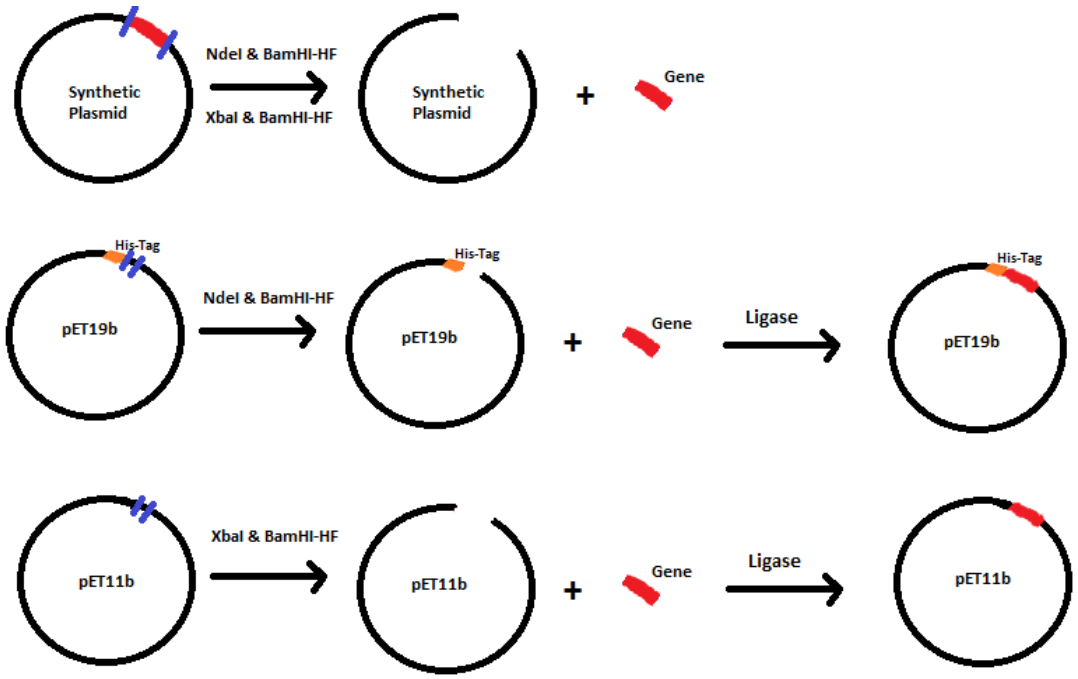

Figure 10. Schematic of SaPGPase subcloning. SaPGPase subcloned into pET19b and pET11b plasmids.

Once the PGPase gene was subcloned into pET11b and pET19b (His•Tag), the PGPase was overexpressed and purified. Production of protein was accomplished by overexpression in *E. coli* (DE3) by induction with IPTG. The cells were lysed via freeze-thaw (untagged protein) or sonication (His•Tagged protein). This was followed by Ni-NTA affinity chromatography for the His•Tagged protein and size exclusion chromatography for both proteins.

Ni-NTA affinity chromatography exploits the fact that nickel readily binds to imidazole (the R group of histidine)[47]. By creating an enzyme with a poly-histidine tag, the enzyme will bind to the Ni-NTA resin, allowing other proteins to pass through the column and isolating the His•Tagged protein. By increasing the imidazole concentration of the solution, the imidazole can outcompete and displace the His•Tagged protein from the column. The sample is dialyzed to remove free imidazole. Dialysis separates molecules based on molecular size; the membrane of the dialysis cassette allows small molecules to passively diffuse through the membrane following a concentration gradient while blocking larger (macro)molecules. A "stepwise" approach was

utilized to lower the imidazole concentration slowly to avoid protein denaturation and precipitation.

In size exclusion chromatography, also known as gel filtration chromatography, a column filled with porous beads is used to separate macromolecules based on molecular weight[48]. Smaller molecules are able to enter the porous beads; as such, their passage through the column is ultimately slowed down. Since larger molecules are unable to enter the beads, they move quickly around the beads and thus move through the column at a faster rate. Not only does this technique readily separate macromolecules according to size, but this technique can also be used to approximate the molecular weight of the macromolecules in a sample[48].

Once the *S. aureus* PGPase was purified, it could be characterized for substrate specificity and conditions for optimal activity including pH optimum and divalent metal ion requirements. These parameters were evaluated by the Ames assay, a colorimetric enzyme assay. In the Ames assay, ammonium molybdate reacts with inorganic phosphate that is released by the enzymatic activity of the PGPase to form a blue phosphomolybdo complex[49]. The intensity of the resulting blue complex is proportional to the concentration of inorganic phosphate, where 50 nmols of phosphate per mL will yield 1 OD at 780 nms[49].

The final component to this project was to determine the kinetic values of the PGPase. This included determining the V_{max}, k_{cat}, K_m, and k_{cat}/K_m for the enzyme with 2-phosphoglycolate or p-nitrophenyl phosphate as the substrate. Additionally, purified PGPase from *S. aureus* was sent to our collaborator, Dr. Roger Rowlett (Colgate University), for x-ray crystallography structure determination.

II. Materials and Methods

i. Synthetic Gene Design

A synthetic gene was designed for the PGPase gene (*sav0929*) from *S. aureus* and the plasmid containing the gene (pMAT-SaPGPase) was ordered from Life Technologies. Two silent mutations were introduced into the gene to remove internal restriction sites. T381C removes an NdeI site and G387A removes a HindIII site. An XbaI restriction site was added to the 5' end of the gene, while a BamHI restriction site was added to the 3' end of the gene, followed by a HindIII site. This gene was delivered in a plasmid (pMAT-SaPGPase) containing an ampicillin resistance gene for selection. ~5 μg of lyophilized DNA was dissolved in 50 μL cold, sterile water and incubated overnight at 4 °C.

ii. Transformations of pMAT-SaPGPase

1 μL of pMAT-SaPGPase was added to 50 μL DH5α (Novagen) competent cells. 5 μL of pUC19 was added to one tube as the positive control. Samples were incubated on ice for 30 minutes followed by a 25 second heat shock in a 37 °C water bath. Immediately following, the samples were placed on ice for at least two minutes. 1 mL of sterile LB media was added to each sample and incubated in a 37 °C water bath for 1 hour, with mixing by inversion every ten minutes. The cells were plated on LB plates containing 0.1 mg/mL ampicillin and incubated at 37 °C for ~16 hours. One colony was streaked to single colonies and one single colony was suspended in LB media containing 0.1 mg/mL ampicillin at 37 °C until 1.0 -1.5 OD (A_{600}). A freezer stock was made from the cell culture by the addition of 0.4 mL 80% glycerol to 1.6 mL of cell culture and stored at -80 °C.

iii. Plasmid Midiprep

E. coli DH5α cells containing pET11b, pET19b, or pMAT-SaPGPase were each grown in 50 mL of LB media containing 0.1 mg/mL ampicillin at 37 °C with shaking for ~16 hours. The cells were harvested (12 tubes containing 3 mL culture) by centrifugation at 16,000 RCF (relative centrifugal force) for 2 minutes at room temperature. Each tube of harvested cells were resuspended in 100 μL of solution I (50 mM glucose, 25 mM Tris•HCl (pH 8.0), and 10 mM EDTA). 200 μL of solution II (0.2 M sodium hydroxide and 1% SDS) was added to lyse the cells. 150 μL of solution III (containing 3 M potassium and 5 M acetate) was used to precipitate *E. coli* chromosomal DNA, leaving the plasmid DNA in solution.

DNase-free bovine pancreatic RNase A (Sigma) in TE buffer (10 mM Tris•HCl (pH 8.0), 1 mM EDTA) was added to the supernatant for a final concentration of 50 μg/mL RNase A, and this was incubated at 37 °C for 30 minutes. Proteins were denatured and removed using a phenol:chloroform (1:1) followed by a chloroform extraction. The plasmid DNA was precipitated with 70% ethanol by freezing the solution (-72 °C) followed by centrifugation at 16,000 RCF at 4 °C for 30 minutes. The pellet, containing the plasmid DNA, was washed with ice-cold 70% ethanol and dried using vacuum centrifugation. The pellet was dissolved in cold sterile water. The plasmid DNA was precipitated with 13% polyethylene glycol (PEG) and 5 M sodium chloride (on ice for approximately 18 hours) leaving tRNAs in the solution. The sample was centrifuged at 16,000 RCF at 4 °C for 30 minutes, and the pellet containing the plasmid was washed with ice-cold 70% ethanol. Pellets were resuspended in cold sterile water. The plasmid DNA concentration was determined by absorbance at 260 nm with a UV-Vis spectrophotometer. The plasmid DNA was analyzed further by 0.7% agarose gel electrophoresis.

iv. Restriction Enzyme Digests

The PGPase synthetic gene was excised from 5000 ng pMAT-SaPGPase plasmid by digestion with 40 units each XbaI and BamHI-HF or 40 units each NdeI and BamHI-HF restriction enzymes (New England Biolabs). 5000 ng pET11b was digested using 40 units each XbaI and BamHI-HF restriction enzymes, while 5000 ng pET19b was digested using 40 units each NdeI and BamHI-HF restriction enzymes. Each plasmid was also digested with each of the enzymes separately to verify efficiency. The double-digestion reactions were incubated at 37 °C for 2 hours. The success of the digestions were verified by gel electrophoresis of the samples that were digested with each individual enzyme, separately. The double-digested samples were gel purified using the protocol in the GeneClean kit (MPBiomedicals). The final concentrations of the digested plasmids were estimated by comparing to molecular weight markers and plasmid standards via agarose gel electrophoresis.

v. Ligation

The PGPase synthetic gene, with digested ends, was ligated into pET11b and pET19b plasmids, to create pETSaPGPase and pET19SaPGPase, respectively, using 0.5 units T4 DNA ligase (Invitrogen) at 15 °C for 24 hours. The ratio of plasmid to gene was varied (Table 1), with a 1:1 ratio theoretically being preferred. Ligations contained digested plasmid, digested gene, ligase buffer, and ligase.

Table 1: Ligations of SaPGPase into pET11b or pET19b.

	Ligation Mixture	Ratio (plasmid:gene)	pET11b[a] (ng)	pET19b[b] (ng)	SaPGPase[c] (ng)
pET11b	**A**	1:0	150	-	0
	B	2:1	150	-	11
	C	1:1	150	-	22
	D	1:2	150	-	44
	E	1:4	150	-	88
pET19b	**F**	1:0	-	150	0
	G	2:1	-	150	11
	H	1:1	-	150	22
	I	1:2	-	150	44
	J	1:4	-	150	88
pUC	--	--	--	--	--

[a]: pET11b is 5676 basepairs
[b]: pET19b is 5717 basepairs
[c]: Sa PGPase is 3208 basepairs

vi. Transformation of *E. coli* DH5α with pETSaPGPase and pET19SaPGPase

E. coli DH5α competent cells were transformed with the ligation mixtures (A-J) and grown on LB plates containing 0.1 mg/ mL ampicillin for 16 hours at 37 °C. *E. coli* DH5α competent cells transformed with pUC19 was used as a positive control. 5 μL of each ligation mixture was added to 50 μL of DH5α *E. coli* competent cells, separately. Samples were incubated on ice for 30 minutes followed by a 25 second heat shock in a 37 °C water bath. Immediately following, the samples were placed on ice for at least two minutes. 1 mL of sterile LB media was added to each sample and incubated in a 37 °C water bath for 1 hour, with mixing by inversion every ten minutes. The cells were plated on LB plates containing 0.1 mg/mL ampicillin and incubated at 37 °C for ~16 hours.

vii. Plasmid miniprep

Colonies from each plate were selected to produce cell cultures from which to analyze the cloned plasmids. Twelve to twenty-four different cultures containing a single colony were grown separately in 5 mL LB media containing 0.1 mg/mL ampicillin at 37 °C with shaking for ~16 hours. 3 mL of each cell culture were harvested by centrifugation at 16,000 RCF at room temperature for 2 minutes. Harvested cells were resuspended with solution I, lysed with solution II, and *E. coli* chromosomal DNA was precipitated with solution III (solutions are the same as above in the midiprep procedure). Phenol:chloroform (1:1) followed by chloroform extractions denatured and removed proteins. The plasmid DNA was precipitated with 70% ethanol by freezing and centrifuging. The pellets were rinsed with ice-cold 70% ethanol, dried by vacuum centrifugation, and resuspended in sterile TE buffer (10 mM Tris•HCl (pH 8.0), 1 mM EDTA) containing 20 μg/mL DNase-free bovine pancreatic RNase A (Sigma). The purified plasmids were analyzed by 0.7% agarose gel electrophoresis; the size of the purified plasmids were compared to purified pET11b or pET19b to determine if their bands ran slower on the gel and thus potentially contained the gene of interest.

viii. Verification of subcloning

In order to verify that the gene was successfully cloned (creating pETSaPGPase and pET19SaPGPase), the miniprepped samples were digested with restriction enzymes. 8 μL of purified plasmid was digested with 20 units of each enzyme (either XbaI and BamHI-HF for pETSaPGPase or NdeI and BamHI-HF). An additional digest using 40 units of EcoRV was carried out for both pETSaPGPase and pET19SaPGPase. All reactions were carried out for 1 hour in a 37 °C water bath. All enzymes were added just prior to incubation. These reactions were analyzed by gel electrophoresis. The double-digests would excise the gene from the

plasmid. The single digest would cut the plasmids in two locations; the resulting bands would differ if there was an inserted gene present. The predicted number and size of fragments was determined. In this way, the ligations were confirmed.

The cell cultures that appeared to contain the successfully cloned gene were streaked to single colonies on LB plates containing 0.1 mg/mL ampicillin and incubated at 37 °C for ~16 hours. One colony from each of a few select plates was picked to produce individual cell cultures by incubating them in LB media containing 0.1 mg/mL ampicillin at 37 °C until 1.0-1.5 OD (A_{600}) was reached. Individual freezer stocks were made from these cell cultures by the addition of 0.4 mL 80% glycerol to 1.6 mL of cell culture and stored at -80 °C.

ix. Sequencing

Samples of pETSaPGPase and pET19SaPGPase purified from the -80 °C freezer stocks by the midiprep procedure were sent to GENEWIZ for sequencing. Standard T7 promoter or T7 terminator primers were used as the primers. The resulting sequences were analyzed using Serial Cloner to ensure the plasmids were correct.

x. Transformation into BLR (DE3)

After confirmation of the success of the subcloning via sequencing, *E. coli* BLR(DE3) competent cells were transformed with purified pETSaPGPase and pET19SaPGPase, separately. The transformed cells were plated onto LB plates containing 0.1 mg/mL ampicillin and incubated at 37 °C for ~16 hours. Colonies were streaked to single colonies, which were used to produce cell cultures (single colonies in LB media containing 0.1 mg/mL ampicillin at 37 °C until 1.0 -1.5 OD (A_{600})). Individual freezer stocks were made from these cell cultures by the addition of 0.4 mL 80% glycerol to 1.6mL of cell culture and stored at-80 °C.

xi. Overexpression of SaPGPase and SaPGPase(HT) in BLR(DE3)

An inoculum of pETSaPGPase in *E. coli* BLR(DE3) was made by adding a scraping of the freezer stock to 7.5 mL LB media containing 0.1 mg/mL ampicillin. The cell culture was grown at 37 °C with shaking until the culture reached ~1.0-1.5 OD (A_{600}). 5 mL of inoculum was added to prewarmed 50 mL LB media, containing 0.1 mg/mL ampicillin, and incubated at 37 °C with shaking to a cell density of ~1 OD (A_{600}). 40 mL of the 50 mL inoculum was added to prewarmed 1L LB media containing 0.1 mg/mL ampicillin. The cell density was analyzed (A_{600}) every 30 minutes until it reached an OD of ~0.8, at which point the culture was induced with 5 mL 50 mg/mL IPTG. Prior to induction, 1.5 mL of culture was harvested and its pellet was labeled TP=0 (Time Point 0) and stored at -80 °C. The induced cells were incubated for 3 hours after induction, with a 1.5 mL sample harvested every hour (TP=1 hr, TP=2 hr, and TP=3 hr). After three hours, the culture was harvested by centrifugation at 1,600 RCF at 4 °C for 15 minutes. The pellet was resuspended in cold buffered saline (50 mM Tris•HCl (pH 7.5), 86 mM NaCl, 67 mM KCl), recentrifuged at 1,600 RCF at 4 °C for 15 minutes, and the pellet rinsed with cold buffered saline. The final pellet was stored at -80 °C.

An inoculum of pET19SaPGPase in *E. coli* BLR(DE3) was made by adding a scraping of the freezer stock to 7.5 mL LB media containing 0.1 mg/mL ampicillin. The cell culture was grown at 37 °C with shaking until the culture reached ~1.0-1.5 OD (A_{600}). 5 mL of inoculum was added to prewarmed 50 mL LB media, containing 0.1 mg/mL ampicillin, and incubated at 37 °C with shaking to a cell density of ~1 OD (A_{600}). 40 mL of the 50 mL inoculum was added to prewarmed 1L LB media containing 0.1 mg/mL ampicillin. The cell density was analyzed every 30 minutes (A_{600}) until it reached an OD of ~0.3, at which point the culture was incubated at 15 °C with shaking to an OD of ~0.6. At this point, the culture was induced with 5 mL 50 mg/mL

IPTG. Prior to induction, 1.5 mL of culture was harvested and its pellet was labeled TP=0 (Time Point 0) and stored at -80 °C. The induced cells were incubated at 15 °C with shaking for an additional ~24 hours. After ~24 hours, 1.5 mL culture was harvested (TP=24 hr). The rest of the culture was harvested by centrifugation at 1,600 RCF at 4 °C for 15 minutes. The pellet was resuspended in cold buffered saline, recentrifuged at 1,600 RCF at 4 °C for 15 minutes, and the pellet rinsed with cold buffered saline. The final pellet was stored at -80 °C.

xii. Purification of SaPGPase from BLR(DE3)

a. Freeze-Thaw purification

The frozen pellet (stored at -80 °C) from the 1 L overexpression was thawed and resuspended in 2 volumes (by weight) TED buffer (50 mM Tris•HCl (pH7.5), 1mM EDTA, 0.1 mM DTT). The freeze-thawed sample was centrifuged at 9,100 RCF for 20 minutes at 4 °C. The supernatant was separated from the pellet. The pellet was resuspended in the same volume of TED buffer, frozen, thawed and centrifuged. The freeze-thawed supernatants were pooled together (~8.0 mL) and ammonium sulfate was added to a final concentration of 80%. The sample was centrifuged at 14,200 RCF for 30 minutes at 4 °C. The supernatant was decanted and the pellet resuspended in 1 mL TED buffer.

b. Size exclusion chromatography

A S-100 sephacryl HR column (3 cm diameter × 80 cm length) was poured and equilibrated with 400 ml buffer A (250 mM NaCl, 50 mM Tris•HCl (pH 7.5), 1mM EDTA, 0.1 mM DTT). The concentrated, partially purified SaPGPase was loaded onto the column and proteins were eluted with 200 ml buffer A, while collecting 2 mL fractions. A_{280}/A_{260} was measured for each fraction. The collected 2 ml fractions were analyzed for PGPase activity by an enzyme assay with p-nitrophenyl phosphate (pNpp), a substrate-analog: in eppendorf tubes, 1 µL of the fraction

was added to 1 μL of 1M MES•NaOH (pH 6.0), 1 μL 100 mM $MgCl_2$, 1 μL 100 mM pNpp, and 6 μL H_2O; the fractions that caused the reactions to produce p-nitrophenol became yellow in color. Those fractions containing enzymatic activity were examined by SDS-PAGE. Those fractions containing "visually" pure SaPGPase were pooled together. The protein in the pooled sample was precipitated with 80% ammonium sulfate and centrifuged at 14,200 RCF for 20 minutes at 4 °C. The supernatant was separated from the pellet and the pellet containing SaPGPase was resuspended in 500 μL TED buffer.

xiii. Purification of SaPGPase(HT) in BLR(DE3)

a. Cell lysis by sonication

The pellet from the 1 L overexpression was resuspended in 2 volumes (by weight) 20 mM Tris•HCl (pH 8.0), placed back at -80 °C for at least one hour and thawed, to assist in cell lysis. Cells were lysed by sonication using a Branson sonicator (output of 6.5 and 50% duty cycle), in 15-second intervals for a total of 10 minutes. Sonicated samples were centrifuged at 14,200 RCF for 30 minutes at 4 °C. The supernatant was separated from the pellet, and each was labeled as sonicated supernatant or sonicated pellet, respectively. Pellets were resuspended in 2 volumes of 20 mM Tris•HCl (pH 8.0). All fractions (whole cell crude extract, sonicated supernatant, and sonicated pellet) were stored at -80 °C.

b. Ni-NTA His•Tag affinity chromatography

Twenty milliliters of Ni^{2+} affinity resin (Novagen) suspension was added to a column (Biorad) and rinsed with ~200 mL binding buffer (5 mM imidazole, 20 mM Tris•HCl (pH 8.0), 500mM NaCl). The sonicated supernatant was loaded onto the column, and 100 mL wash buffer (60 mM imidazole, 20 mM Tris•HCl (pH 8.0), 500 mM NaCl) was used to elute all of the *E. coli* proteins, leaving the His•Tagged SaPGPase protein bound to the resin. The column was rinsed

with 50 mL elute buffer (250 mM imidazole, 20 mM Tris•HCl (pH 8.0), 500 mM NaCl) to elute 2 mL fractions containing the His•Tagged SaPGPase protein. The protein concentration of each fraction was determined by a Bradford assay and the fractions containing protein were analyzed by SDS PAGE.

Fractions containing the His•Tagged SaPGPase protein and devoid of most other proteins were combined and dialyzed using a Slide-A-Lyzer (10 kD MWCO) cassette (Pierce). A "step down" dialysis procedure was used: dialysis in buffer 1 (100 mM imidazole, 250 mM NaCl, 20 mM Tris•HCl (pH 7.5)), followed by buffer 2 (50 mM imidazole, 250 mM NaCl, 20 mM Tris•HCl (pH 7.5)) each for 1 hour, followed by buffer 3 (250 mM NaCl, 50 mM Tris•HCl (pH 7.5), 1 mM EDTA, 0.1 mM DTT) overnight. This dialysis process was necessary to avoid protein denaturation and precipitation. The dialyzed protein solution was concentrated using Amicon Ultra Centrifugal filter units (Millipore) centrifuged at 2,300 RCF at 4 °C until the final volume was ~0.5-1.0 mL.

c. Size exclusion chromatography

A S-100 sephacryl HR column was prepared as described above. SaPGPase(HT) was loaded onto the column and proteins were eluted with 200 ml of buffer A, while collecting 2 mL fractions. Fractions were analyzed for SaPGPase(HT) as described above. Those fractions containing enzymatic activity were examined by SDS-PAGE. Those fractions containing "visually" pure SaPGPase(HT) were pooled together. The pooled protein solution was concentrated using Amicon Ultra Centrifugal filter units (Millipore) centrifuged at 2,300 RCF at 4 °C until the final volume was ~1.0 mL.

xiv. Analysis of protein purification

a. SDS PAGE analysis

All time point samples were resuspended in H_2O (100 μL per OD). Each whole cell crude extract, freeze-thawed supernatant, freeze-thawed pellet, sonicated supernatant, and sonicated pellet was diluted to 0.1x with 20 mM Tris•HCl (pH 8.0). 5 μL of each time point or 0.1x sample, 10 μL 20 mM Tris•HCl (pH 8.0), and 5 μL 4x protein loading buffer (200 mM Tris•HCl (pH 6.8), 40% glycerol, 8% SDS, 400 mM DTT, and 0.08% bromophenol blue dye) were mixed together and boiled for 10 minutes. The samples were analyzed by SDS PAGE (100 V for 20 minutes followed by 300 V for ~30-35 minutes). The gel was stained with Coomassie blue dye, and de-stained with destain I (45% methanol, 9% acetic acid) for ~10 minutes followed by destain II and Kimwipes (10% methanol and 10% acetic acid) overnight. The gel was placed in drying solution (30% methanol and 5% glycerol) for 1 hour, and dried between cellophane membranes.

b. Bradford assay

Solution containing protein (typically 5-20 μL) was added to 800 μL of water and mixed well. To this mixture, 200 μL Bradford dye (BioRad) was added. Protein concentration was determined by measuring A_{595} and using a standard curve of A_{595} as a function of BSA concentration (see appendix).

xv. Enzyme characterization

a. Determination of specific activity

The standard reaction mixture contained 50 mM MES•NaOH (pH 6.0), 10 mM $MgCl_2$, 1 mM DTT and either 4 mM pNpp or 4 mM 2-phosphoglycolate (2-PG) in 50 µl. Reactions with varying enzyme amounts were carried out for 30 min at 37 ºC and quenched with 250 µl 4 mM EDTA. Diluent (1 mg/mL BSA, 10% glycerol, 50 mM Tris (pH7.5), 1 mM DTT, and 1 mM EDTA) was used in place of the enzyme in the negative control. The Ames and Dubin colorimetric assay[49] was used to measure the concentration of inorganic phosphate released by the enzyme. Briefly, 600 µL 0.42% ammonium molybdate in 1 N H_2SO_4 mixed with 100 µL 10% ascorbic acid was added to 300 µL quenched reaction mixture. This 1 mL mixture was incubated at 42 °C for 20 minutes and blue ammonium-molybdo-phospho complex was measured at A_{780}. Phosphate was quantified by: 50 nmol phosphate yields 1 OD at A_{780}.

b. pH optimization

The standard reaction mixture consisted of 50 µl of 10 mM $MgCl_2$, 1 mM DTT and 4 mM pNpp or 4 mM 2-PG. 50 mM acetate (pH 4-5.5) 50 mM MES•NaOH (pH 5.0-7.0), or 50 mM glycine (pH 8.0-10.0) were added to determine the pH optimum of the enzymatic reaction. Reactions with varying enzyme concentrations were carried out for 30 minutes at 37 ºC and quenched with 250 µl 4 mM EDTA. The Ames and Dubin colorimetric assay[49] was used to measure the concentration of inorganic phosphate released by the enzyme, as described above.

c. Metal ion preference

The standard reaction mixture consisted of 50 µl of 50mM MES•NaOH (pH 6.0) with 1 mM DTT and 4 mM pNpp or 4 mM 2-PG. $MgCl_2$, $MnCl_2$, $ZnCl_2$, $CaCl_2$ or $CoCl_2$ were added to 1mM or 10 mM divalent metal ion concentrations. Reactions were carried out for 30 minutes at

37 ºC and quenched with 250 µl 4 mM EDTA. The Ames and Dubin colorimetric assay[49] was used to measure the concentration of inorganic phosphate released by the enzyme, as described above.

d. Metal ion concentration optimization

Enzyme assays were carried out for solutions with concentrations of $MgCl_2$ ranging from 1 mM to 50 mM. The standard reaction mixture consisted of 50 µl of 50 mM MES•NaOH (pH 6.0), 1 mM DTT and 4 mM pNpp or 4 mM 2-PG. Varying concentrations of $MgCl_2$ were used for each of the reaction mixtures. The reactions were carried out for 30 minutes at 37 ºC and quenched with 250 µl 20 mM EDTA. Note that more EDTA was needed in these assays to chelate the larger concentrations of Mg^{2+}. The Ames and Dubin colorimetric assay[49] was used to measure the concentration of inorganic phosphate released by the enzyme, as described above.

e. Substrate specificity

The standard reaction mixture consisted of 50 µl of 50mM MES•NaOH (pH 6.0), 10 mM $MgCl_2$, and 1 mM DTT. 2 µL 100 mM substrate was chosen from a substrate library stored at -80 °C (Table 2). Reactions were carried out for 30 minutes at 37 ºC and quenched with 250 µl 4 mM EDTA. The Ames and Dubin colorimetric assay[49] was used to measure the concentration of inorganic phosphate released by the enzyme, as described above.

Table 2: Substrates used to determine enzyme specificity

2,3-diphosphoglycerate	Histidine phosphate	p-nitrophenly phosphate
2-phosphoglycerate	Mannose-1-phosphate	Pyridoxamine Phosphate
2-Phosphoglycerol	Mannose-6-phosphate	Ribose-5-phosphate
2-phosphoglycolate	NADP	Ribulose-5-phosphate
3-phosphoglycerate	NADPH	Thiamine diphosphate
3-phosphoglycerol	NAG-1-phosphate	Thiamine monophosphate
Arabinose-5-phosphate	NAG-6-phosphate	Thiazole phosphate
DHAP	o-Phospho-L-Arginine	Trehalose-6-phosphate
Fructose-1,6-bisphosphate	o-Phospho-L-Serine	Phosphoribosyl pyrophosphate
Fructose-1-phosphate	o-Phospho-L-Threonine	dCMP
Fructose-2,6-bisphosphate	o-Phospho-L-Tyrosine	dAMP
Fructose-6-phosphate	phosphoenolpyruvate	dGMP
Glucosamine-1-phosphate	phosphocreatine	dTMP
Glucosamine-6-phosphate	phosphoinositides	CMP
Glucose-1,6-bisphosphate	phosphoinositol	AMP
Glucose-1-phosphate	phosphoryl ethanolamine	GMP
Glucose-6-phosphate	phosphorylcholine	UMP
Glyceraldehyde phosphate	Pyridoxal phosphate	

f. Kinetics

Enzyme assays were carried out for reactions with 0.1 mM to 40 mM pNpp or 0.1 mM to 20 mM 2-PG. The standard reaction mixture consisted of 50 µl of 50mM MES•NaOH (pH 6.0), 10 mM $MgCl_2$, and 1 mM DTT. The reactions were carried out for 30 minutes at 37 ºC and quenched with 250 µl 4 mM EDTA. The Ames and Dubin colorimetric assay[49] was used to measure the concentration of inorganic phosphate released by the enzyme, as described above. The results were used to generate nonlinear regression and Lineweaver-Burke plots. Kinetic values were determined using the program EnzymeKinetics.

III. Results and Discussion

i. Plasmid Purification

The pMAT-SaPGPase, pET19b, and two samples of the pET11b plasmids were purified from *E. coli* DH5α competent cells. Two samples of pET11b were purified due to lower yield. Upon purification, the quantities of the purified plasmids (Table 3) were determined by the following equation:

$$\text{DNA concentration (ng/μL)} = A_{260} * \frac{50\ \mu g/mL}{1\ OD} * dilution\ factor$$

Table 3: Quantification of pMAT-SaPGPase, pET19b, and pET11b.

Plasmid	**[DNA]** (ng/μL)	**Volume** (μL)	**DNA** (μg)
pMAT-SaPGPase	365	120	40
pET19b	255	120	31
pET11b	125	120	15
pET11b	130	120	16

Plasmid purity is displayed in Figure 11. Previously purified samples of pET11b or pET19b were used as positive controls. The intensity of the bands for the newly purified plasmids are approximately the same as the intensity of the bands for the control plasmids in Figure 11A and 11B, while the intensity of the band for the newly purified plasmid is approximately twice that of the band for the control in Figure 11C. The bands are sharp single bands indicating good purity.

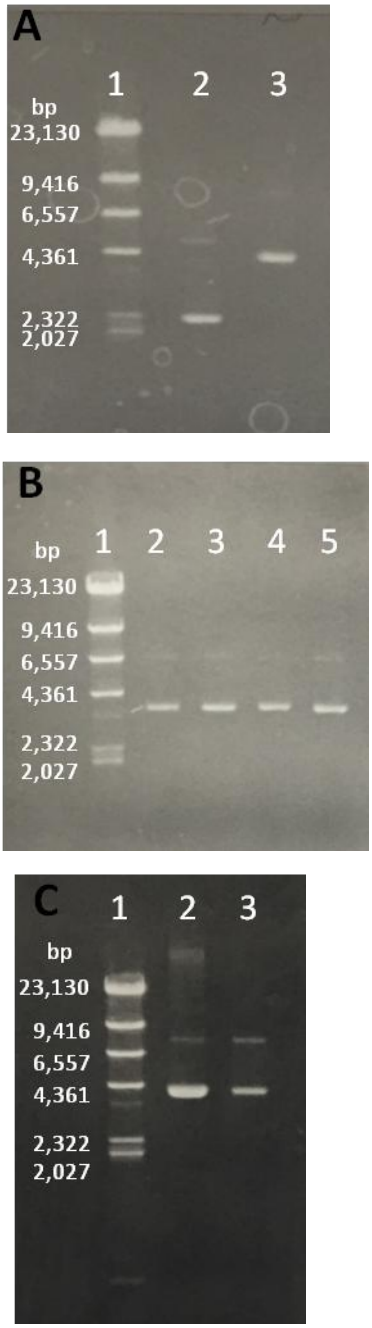

Figure 11: Plasmid midipreps of pMAT-SaPGPase, pET19b, and pET11b. **A**: pMAT-SaPGPas. Lane 1: λ HindIII molecular weight markers (MWM), Lane 2: 100 ng previously purified pET11b, Lane 3: 100 ng pMAT-SaPGPase. **B**: pET19b and pET11b. Lane 1: λ HindIII MWM, Lane 2: 100 ng pET19b, Lane 3: 100 ng of previously purified pET19b, Lane 4: 100 ng previously purified pET11b, Lane 5: 100 ng pET11b. **C**: pET11b. Lane 1: λ HindIII MWM, Lane 2: 100 ng pET11b, Lane 3: 100 ng of previously purified pET11b.

ii. Plasmid Digestion and Purification

The pET11b plasmid and a portion of the pMAT-SaPGPase plasmid were both digested with XbaI and BamHI-HF restriction enzymes while pET19b and another portion of the pMAT-SaPGPase were digested with NdeI and BamHI-HF. These digests excised the PGPase gene from pMAT-SaPGPase and created comparable restriction "sticky ends" on the gene and within the pET plasmids. Single digests of each of the plasmids by the individual restriction enzymes (either NdeI, BamHI-HF, or XbaI) were complete within 1 hour (Figure 12). If the single digests were each complete, then it could be assumed that the double digests were complete as well, since all were carried out under identical conditions. Singly digested pET11b and pET19b plasmids ran on a gel as expected for linear DNA of ~5.7 kbp, while the singly digested pMAT-SaPGPase ran on a gel as expected for linear DNA of ~3.2 kbp.

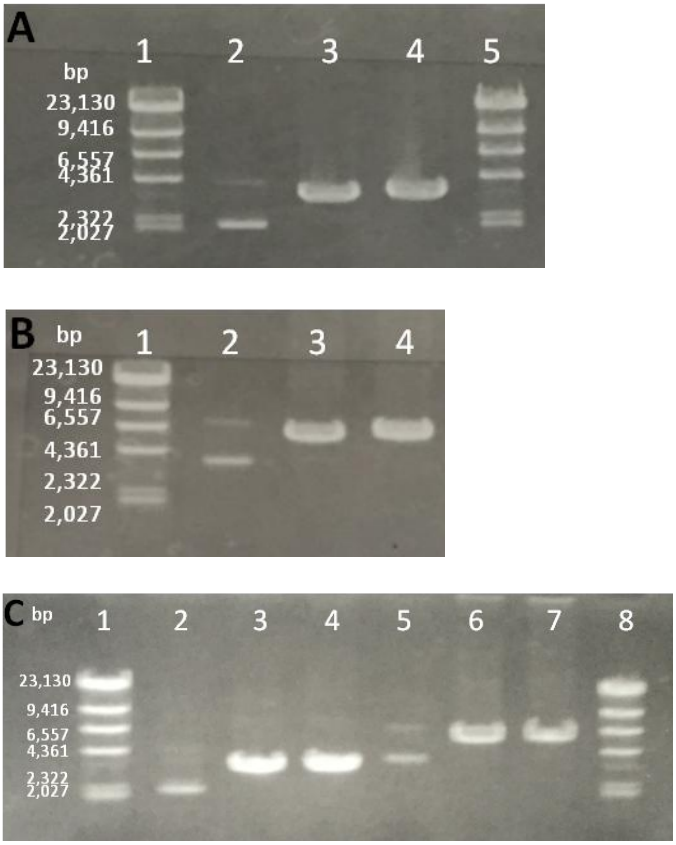

Figure 12: Single restriction digests of pMAT-SaPGPase, pET11b, and pET19b. **A**: pMAT-SaPGPase. Lane 1 & 5: λ HindIII MWM, Lane 2 100 ng pMAT-SaPGPase, Lane 3: pMAT-SaPGPase digested with XbaI, Lane 4: pMAT-SaPGPase digested with BamHI-HF. **B**: pET11b. Lane 1: λ HindIII MWM, Lane 2: 100 ng pET11b, Lane 3: pET11b digested with XbaI, Lane 4: pET11b digested with BamHI-HF. **C**: pMAT-SaPGPase and pET19b. Lane 1 & 8: λ HindIII MWM, Lane 2: 100 ng pMAT-SaPGPase, Lane 3: pMAT-SaPGPase digested with NdeI, Lane 4: pMAT-SaPGPase digested with BamHI-HF, Lane 5: 100 ng pET19b, Lane 6: pET19b digested with NdeI, Lane 7: pET19b digested with BamHI-HF

The double digested samples of pMAT-SaPGPase, pET11b, and pET19b were purified on an agarose gel, and the excised PGPase gene and digested pET11b and pET19b were extracted from the gel and further purified using the GeneClean kit (Figure 13).

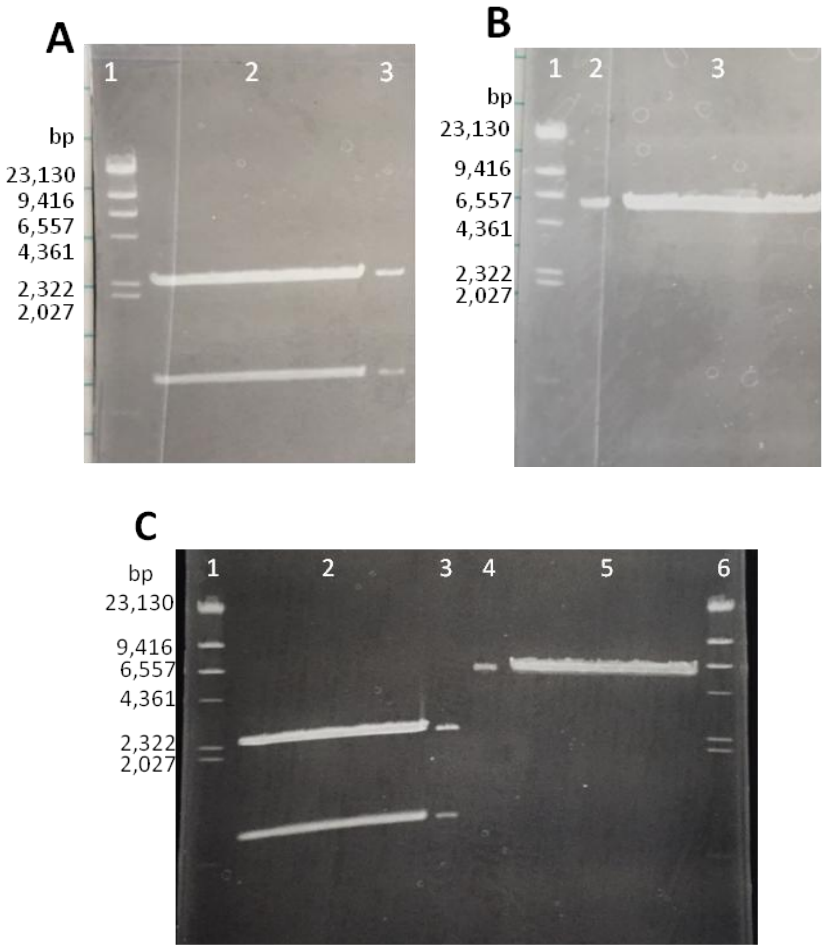

Figure 13: Gel purification of double restriction digests of pMAT-SaPGPase, pET11b, and pET19b. A: pMAT-SaPGPase. Lane 1: λ HindIII MWM, Lanes 2 & 3: pMAT-SaPGPase digested with XbaI and BamHI-HF. **B:** pET11B. Lane 1: λ HindIII MWM, Lanes 2 & 3: pET11b digested with XbaI and BamHI-HF. **C:** pMAT-SaPGPase and pET19b. Lanes 1 & 6: λ HindIII MWM, Lanes 2 & 3: pMAT-SaPGPase digested with NdeI and BamHI-HF, Lanes 4 & 5: pET19b digested with NdeI and BamHI-HF.

The concentrations of the purified digested gene and plasmids were estimated by comparing to standards on agarose gels (Figure 14). The estimated concentrations were as follows: purified digested pET11b was ~150 ng/μL, SaPGPase excised with XbaI and BamHI-HF was ~50 ng/μL, purified digested pET19b was ~150 ng/μL, and SaPGPase excised with NdeI and BamHI-HF was ~50 ng/μL.

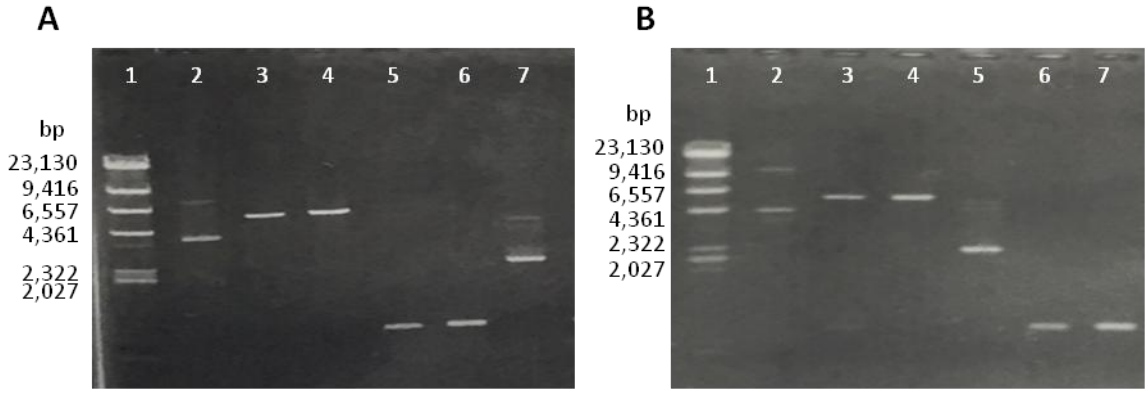

Figure 14: Digested, gel-purified, gene-cleaned pET11b, pET19b, and SaPGPase. A: pET11b and SaPGPase digested with XbaI and BamHI-HF. Lane 1: λ HindIII MWM, Lane 2: 100 ng pET11b, Lane 3: 1 μL digested, gene-cleaned pET11b, Lane 4: 2 μL digested, gene-cleaned pET11b, Lane 5: 1 μL digested, gene-cleaned SaPGPase, Lane 6: 2 μL digested, gene-cleaned SaPGPase, Lane 7: 100 ng SaPGPase. **B:** pET19b and SaPGPase digested with NdeI and BamHI-HF. Lane 1: λ HindIII MWM, Lane 2: 100 ng pET19b, Lane 3: 1 μL digested, gene-cleaned pET19b, Lane 4: 2 μL digested, gene-cleaned pET19b, Lane 5: 100 ng SaPGPase, Lane 6: 1 μL digested, gene-cleaned SaPGPase, Lane 7: 2 μL digested, gene-cleaned SaPGPase.

iii. Ligation and Transformation

Ligations are most efficient when the concentration of plasmid is 10-20 ng/ μL and the ratio of plasmid:gene is 1:1[50]. The size of pET11b and pET19b is ~5.7 kbp, whereas the PGPase gene is ~0.8 kbp. Therefore, if 150 ng of plasmid is used, then 22 ng of gene is required to achieve a 1:1 ratio of plasmid to gene. Because DNA concentrations could only be estimated, as described above, the ratios of plasmid:gene were varied around a 1:1 ratio (see Table 4). Ligations A and F contained only purified digested plasmid and no gene, as negative controls. Any colonies that resulted from these ligations would be due to the re-ligation of plasmid, thus indicating less than

100% cleavage by both restriction enzymes. The number of colonies that resulted from ligated gene into plasmid was up to 450 times greater than ligated plasmid alone for pET11b and approximately double for pET19b. pUC19 was used as a positive control for transformation.

Table 4: Ligations of SaPGPase into pET11b or pET19b.

	Ligation Mixture	**Ratio** (plasmid:gene)	**pET11b**[a] (ng)	**pET19b**[b] (ng)	**SaPGPase**[c] (ng)	**Colonies**[d]
pET11b	**A**	1:0	150	-	0	1
	B	2:1	150	-	11	18
	C	1:1	150	-	22	158
	D	1:2	150	-	44	~450
	E	1:4	150	-	88	~360
pET19b	**F**	1:0	-	150	0	140
	G	2:1	-	150	11	~300
	H	1:1	-	150	22	~315
	I	1:2	-	150	44	~200
	J	1:4	-	150	88	~200
pUC	--	--	--	--	--	Lawn

[a]: pET11b is 5676 basepairs
[b]: pET19b is 5717 basepairs
[c]: SaPGPase is 3208 basepairs
[d]: 50 µL transformed cell cultures on LB-Ampicillin plates.

Twelve colonies from plates B-E were analyzed for successful subcloning of pETSaPGPase and twelve colonies from G-J were analyzed for successful subcloning of pET19SaPGPase. As shown in Figure 15, both pETSaPGPase and pET19SaPGPase were successfully subcloned. Both subclones contain ~6.5 kbp and thus run slower on the agarose gel as compared to the ~5.7 kbp pET11b and pET19b.

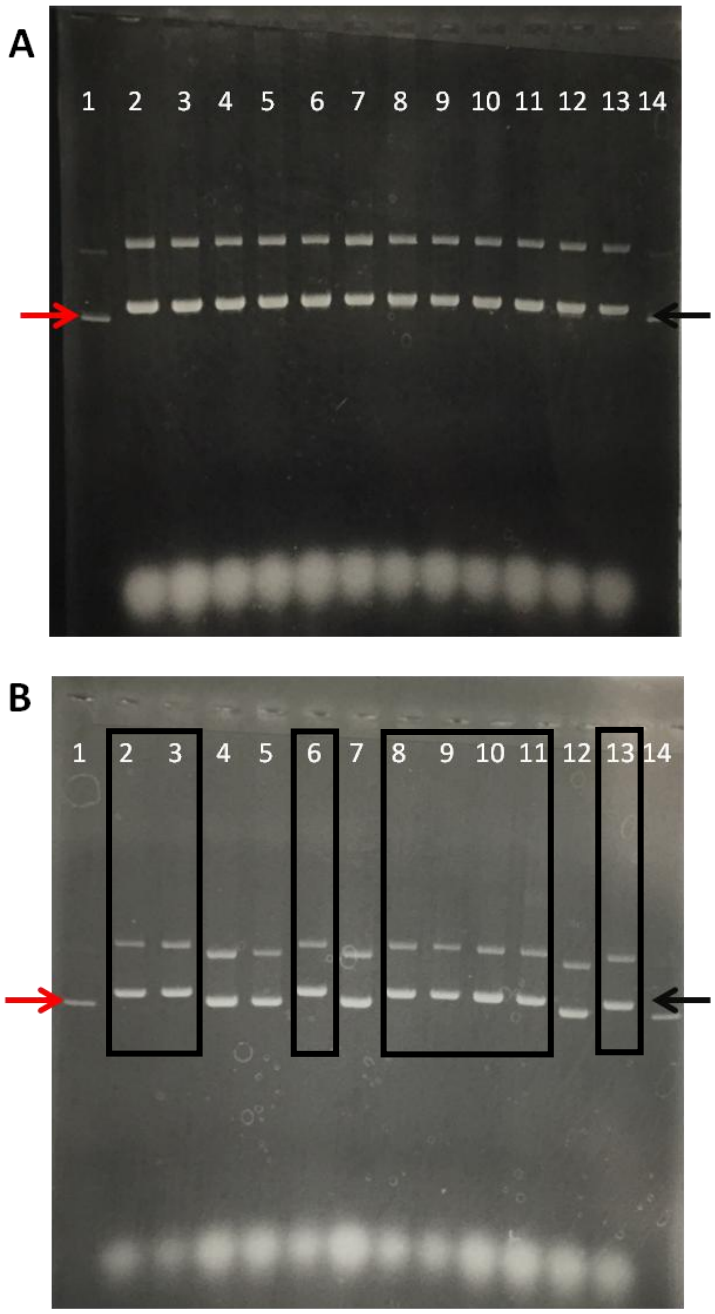

Figure 15: Screening of possible pETSaPGPase and pET19SaPGPase. A: plasmid minipreps for pETSaPGPase. Lanes 1 & 14: 100 ng pET11b, Lanes 2-13: pETSaPGPase. **B:** plasmid minipreps for pET19SaPGPase. Lanes 1 & 14: 100 ng pET19b, Lanes 2,3,6,8-11, and 13 (boxed): pET19SaPGPase. Lanes 4, 5, 7, and 12: religated pET19b. Red arrows on the left side of the images indicate the position of pET11b or pET19b, while the black arrows on the right indicate the position of pETSaPGPase or pET19SaPGPase that have successfully been cloned.

iv. Verification of Subcloning

To verify that pETSaPGPase and pET19SaPGPase were successfully subcloned, EcoRV, XbaI with BamHI-HF, and NdeI with BamHI-HF were used. As shown in Figure 16, EcoRV produced bands of 4229 bp for all plasmids and a second band of either 1447-1488 bp for pET11b/pET19b or 2196-2260bp for pETSaPGPase/pET19SaPGPase, indicating that the PGPase gene of ~780 bp was successfully subcloned into both pET11b and pET19b. When XbaI with BamHI-HF or NdeI with BamHI-HF were used, the enzymes excised the gene from pETSaPGPase and pET19SaPGPase, producing fragments of 833 bp or 783 bp, respectively. The double bands shown in Figure 16B were due to incomplete digestion by NdeI and BamHI-HF.

Table 5: Digestion patterns for pET11b, pET19b, pETSaPGPase, and pET19SaPGPase. using SerialCloner.

	EcoRV (bp)	**XbaI & BamHI-HF** (bp)	**NdeI & BamHI-HF** (bp)
pET11b	4229 + 1447	5599 + 77	------
pETSaPGPase	4229 + 2196	5599 + 822	------
pET19b	4229 + 1488	------	5706 + 11
pET19SaPGPase	4229 + 2260	------	5706 + 783

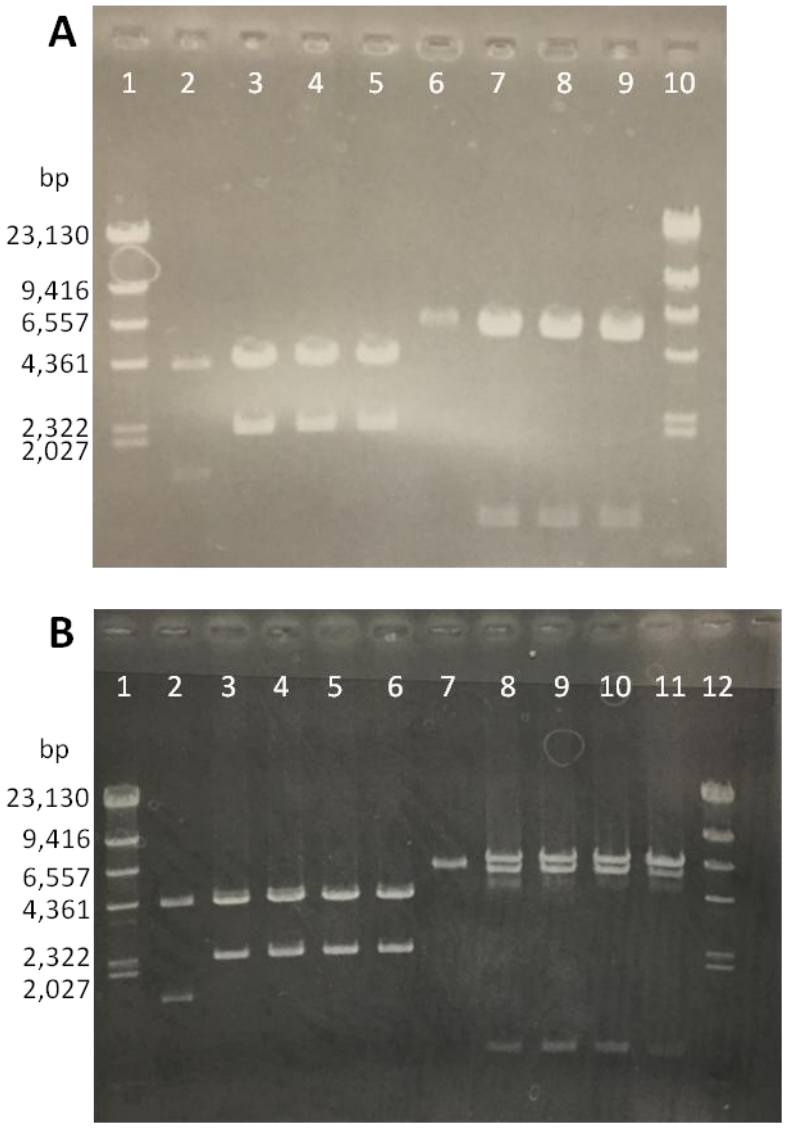

Figure 16: Verification of pETSaPGPase and pET19SaPGPase subcloning. A: pETSaPGPase. Lanes 1 & 10: λ HindIII MWM, Lane 2: pET11b digested with EcoRV, Lanes 3-5: pETSaPGPase digested with EcoRV, Lane 6: pET11b digested with XbaI & BamHI-HF, Lanes 7-9: pETSaPGPase digested with XbaI & BamHI-HF. **B:** pET19SaPGPase. Lanes 1 &12: λ HindIII MWM, Lane 2: pET19b digested with EcoRV. Lanes 3-6: pET19SaPGPase digested with EcoRV. Lane 7: pET19b digested with NdeI & BamHI-HF, Lanes 8-11: pET19SaPGPase digested with NdeI & BamHI-HF.

v. Midiprep of pETSaPGPase and pET19SaPGPase

Midiprep purification was performed to purify pETSaPGPase and pET19SaPGPase from *E. coli* DH5α. The DNA concentration was determined by A_{260} (Table 6). Purity and yield were verified by agarose gel electrophoresis (Figure 17).

Table 6: Quantification of pETSaPGPase and pET19SaPGPase.

Plasmid	**DNA** (ng/μL)	**Volume** (μL)	**DNA** (μg)
pETSaPGPase	235	120	28
pET19SaPGPase	220	120	26

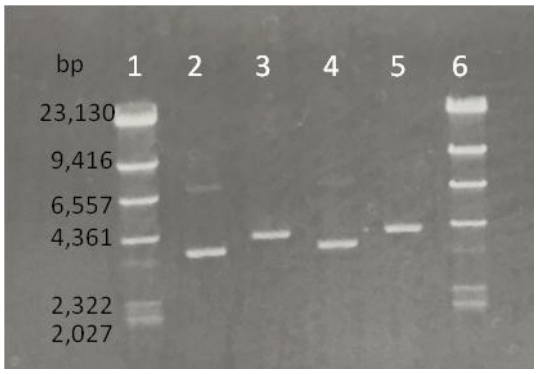

Figure 17: Plasmid midipreps of pETSaPGPase and pET19SaPGPase. Lanes 1 & 6: λ HindIII MWM, Lane 2: 100 ng pET11b, Lane 3: 100 ng pETSaPGPase, Lane 4: 100 ng pET19b, Lane 5: 100 ng pET19SaPGPase

vi. Sequencing of pETSaPGPase and pET19SaPGPase

The sequence of pETSaPGPase and pET19SaPGPase were confirmed to be correct with the incorporated gene sequence matching that of SAV0929 from *S. aureus* Mu50. Once the gene sequence was confirmed, *E. coli* BLR(DE3) was transformed with pETSaPGPase and pET19SaPGPase.

vii. Overexpression of SaPGPase(HT) in *E. coli* BLR (DE3)

S. aureus PGPase(HT) was overexpressed in *E. coli* BLR(DE3) at 15 °C. The cells were harvested 24 hours after induction with IPTG, and sonicated to produce the fractions shown in Figure 18**.** SaPGPase(HT) expression is observed by the appearance of a major band between the 25 and 37 kDa molecular weight markers (MWMs) upon induction. Only ~50% of the SaPGPase(HT) was released from the cells, even after 10 minutes of sonication (either due to protein insolubility or incomplete sonication. However, a sufficient quantity of SaPGPase(HT) was in the sonicated supernatant; the sonicated supernatant contained 170 mg total protein.

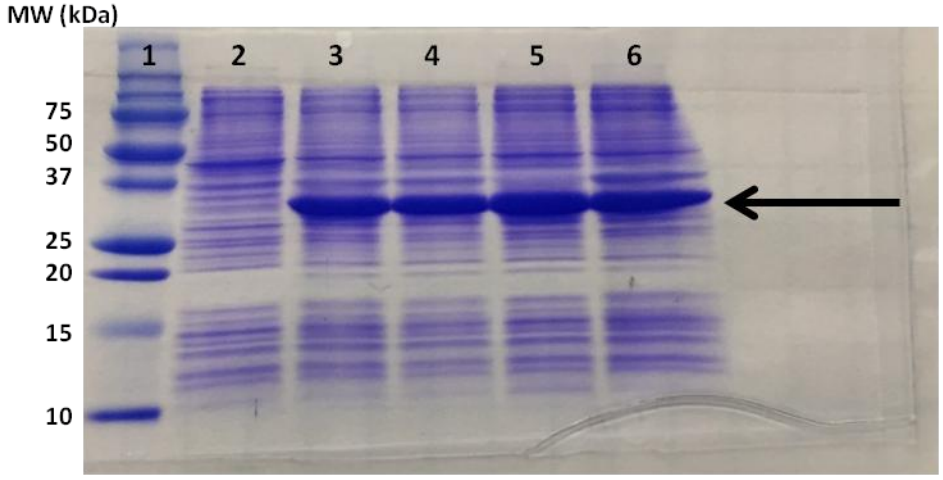

Figure 18: Overexpression and solubility of SaPGPase(HT) from BLR(DE3). Lane 1: MWMs, Lane 2: prior to induction, Lane 3: 24 hours after induction, Lane 4: crude extract, Lane 5: sonicated supernatant, Lane 6: sonicated pellet. The arrow indicates SaPGPase(HT).

viii. Ni-NTA affinity chromatography of *S. aureus* PGPase(HT)

Sonicated supernatant containing SaPGPase(HT) was purified by Ni-NTA affinity chromatography. Using a wash buffer containing 60 mM imidazole, all proteins were eluted from the column with the exception of the SaPGPase(HT) bound to the Ni^{2+} through the ten-histidine tag at the N-terminal end of the protein. The bound protein was eluted from the column by increasing the imidazole concentration to 250 mM (elution buffer). As shown in Figure 19, the SaPGPase(HT) was significantly purified with virtually all other protein eluting with wash buffer and the SaPGPase(HT) eluting within a few fractions with the elution buffer. Elution fractions 5-9 were pooled together and the imidazole was dialyzed out in a stepwise manner as not to denature and precipitate the SaPGPase(HT). After dialysis, the sample was concentrated with an Amicon filter unit (Millipore) to a volume of 1.4 ml with a protein concentration of 33.3 mg/mL for a total of 47 mg protein.

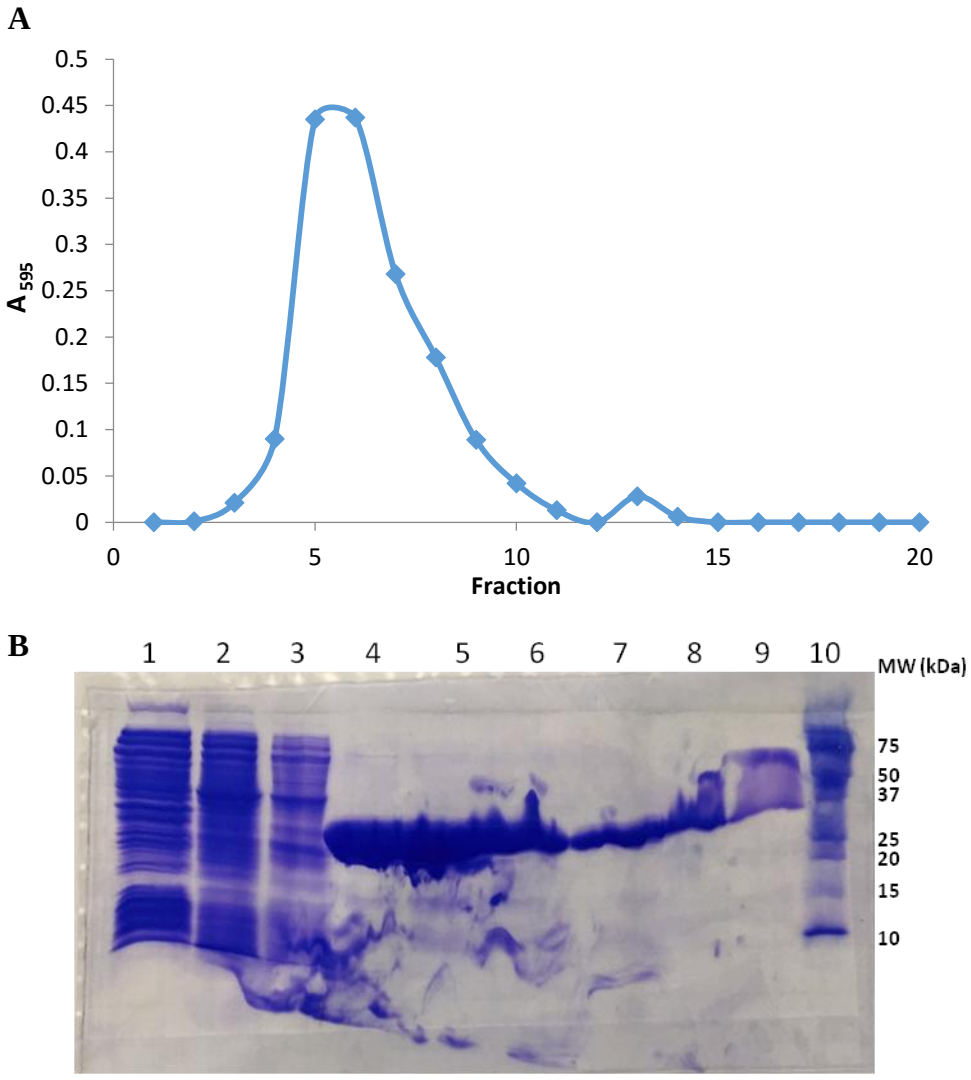

Figure 19: Ni-NTA affinity chromatography of SaPGPase(HT). A: A_{595} (Bradford assay) vs. fraction. **B:** SDS-PAGE. Lanes 1-3: wash fractions 2-4. Lanes 4-9: elution fractions 5-10. Lane 10: MWMs.

ix. Size exclusion chromatography of *S. aureus* PGPase(HT)

Size exclusion chromatography was used to remove any remaining impurities from SaPGPase(HT). Figure 20 shows the analysis of fractions that were eluted from the column. The fractions containing purified SaPGPase(HT) (fractions 58-63) were pooled together and concentrated using an Amicon filter unit (Millipore) to a final volume of 1.4 mL with a protein concentration of 20.6 mg/mL for a total of 29 mg protein). The SaPGPase(HT) eluted from the size exclusion column in fractions that corresponded to a protein standard of 29 kDa, indicative that the SaPGPase(HT), with a monomeric mass of 29.3 kDa, is a monomeric protein in solution (see appendix).

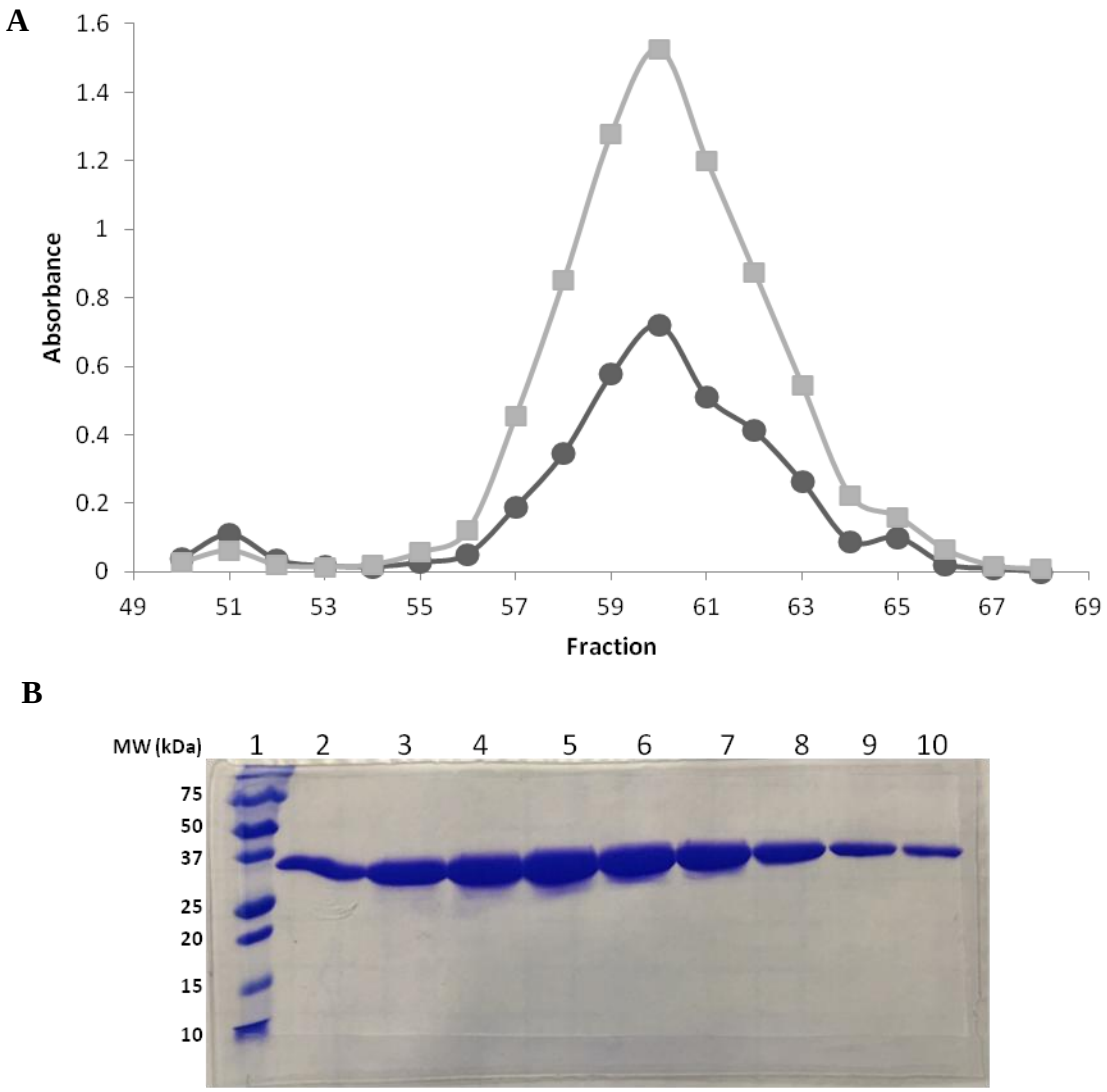

Figure 20: Size exclusion chromatography of SaPGPase(HT). A: Absorbance (● A_{260}, ■ A_{280}) vs. fraction. **B:** SDS-PAGE. Lane 1: MWMs, Lanes 2-10: fractions 57-65.

x. Overexpression of SaPGPase in *E.coli* BLR(DE3)

S. aureus PGPase (without a His•Tag) was overexpressed in *E. coli* BLR(DE3) at 37 °C. The cells were harvested 3 hours after induction with IPTG and underwent two rounds of freezing and thawing to produce the fractions seen in Figure 21**.** SaPGPase expression is observed by the appearance of a major band between the 25 and 37 kDa MWMs upon induction. Approximately 25% of the SaPGPase was released from the cells after one round of freeze-thaw. A second round of freeze-thaw was able to release ~50% of the SaPGPase that remained in the first freeze-thaw pellet. The two freeze-thaw supernatants were pooled together for a protein concentration of 5.75 mg/mL in a volume of 8.0 mL for a total of 46 mg protein.

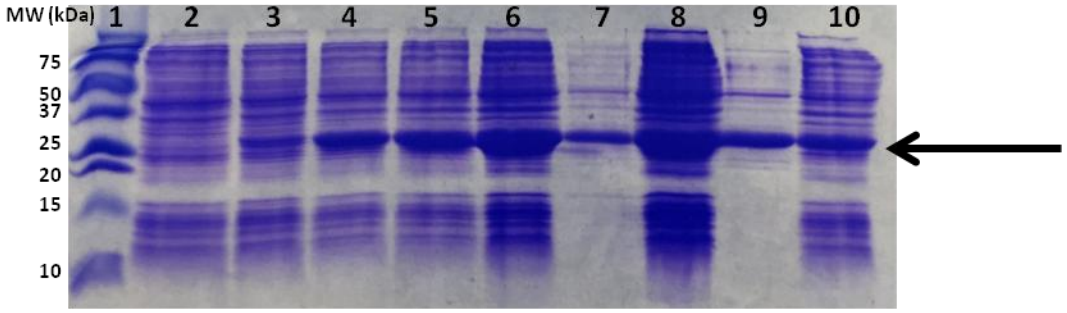

Figure 21: Overexpression and solubility of SaPGPase from BLR(DE3). Lane 1: MWMs, Lane 2: prior to induction, Lane 3: 1 hour after induction, Lane 4: 2 hours after induction, Lane 5: 3 hours after induction, Lane 6: crude extract, Lane 7: freeze-thaw supernatant, Lane 8: freeze-haw pellet, Lane 9: second freeze-thaw supernatant, Lane 10 second freeze-thaw pellet. The arrow indicates SaPGPase.

xi. Ammonium sulfate concentration of SaPGPase

The freeze-thaw extract containing SaPGPase was concentrated by the addition of ammonium sulfate to a final concentration of 80% (Figure 22), causing SaPGPase to precipitate. The precipitant was resuspended in 1 mL TED buffer**.** The final protein concentration was 22.3 mg/mL in a volume of 1.7 mL for a total of 36 mg protein.

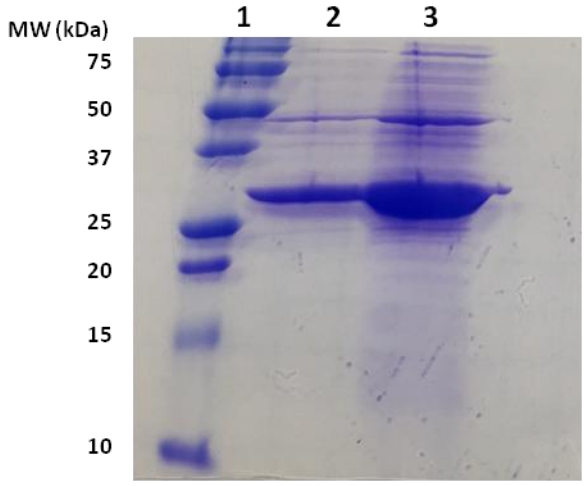

Figure 22: Ammonium sulfate concentration of SaPGPase freeze-thaw extract. Lane 1: MWMs, Lane 2: 1 µL pooled freeze-thaw extract, Lane 3: 1µL of concentrated SaPGPase.

xii. Size exclusion chromatography of SaPGPase

Size exclusion chromatography was used to further purify the SaPGPase protein. Figure 23 shows the analysis of fractions that were eluted from the column. Two separate pooled fractions were concentrated by 80% ammonium sulfate precipitation. The SaPGPase was separated into two fractions due to the presence of another protein. The purer fraction, Fraction A (fractions 53-60) had a final volume of 1.7 mL with a protein concentration of 11.5 mg/mL for a total of 19.5 mg protein, while the less pure fraction, Fraction B (fractions 61-65) had a final volume of 0.6 mL with a protein concentration of 12.4 mg/mL for a total of 7.4 mg protein. As with the SaPGPase(HT), the SaPGPase eluted from the size exclusion column in fractions that corresponded to a protein standard of 29 kDa, indicative that the SaPGPase (with a monomeric molecular mass of 27.9 kDa) is a monomeric protein (see appendix). The SaPGPase was not as pure as the SaPGPase(HT), but its purity sufficed for comparison to the His•Tagged protein.

A

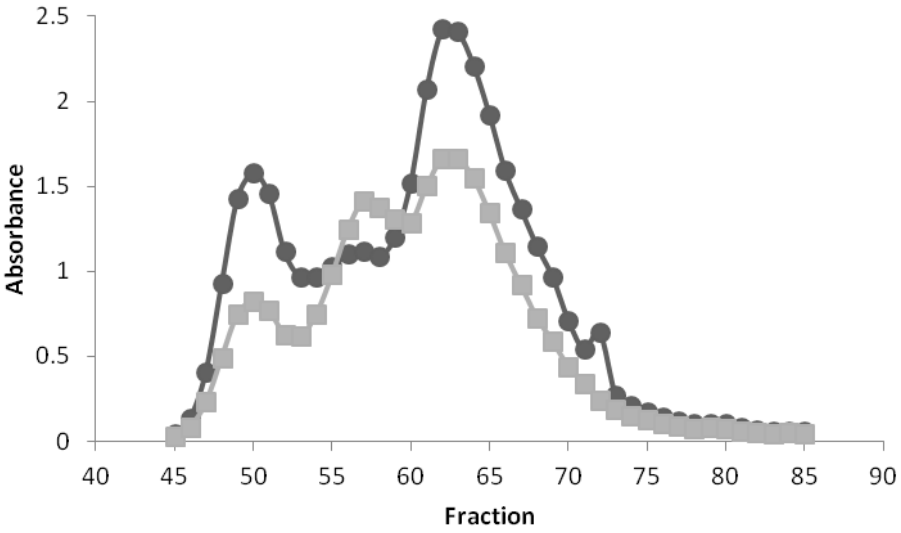

B

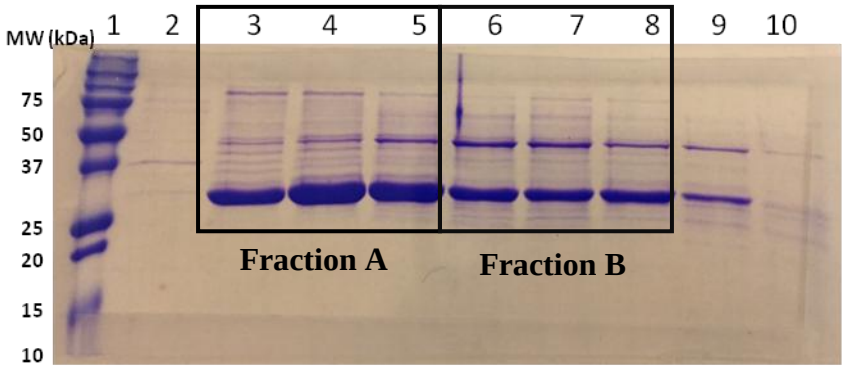

Figure 23: Size exclusion chromatography of SaPGPase. A: Absorbance (● A_{260}, ■ A_{280}) vs. fraction. **B:** SDS-PAGE. Lane 1: MWMs, Lanes 2-10: fractions 50, 55, 57, 59, 61, 63, 65, 68, and 71, respectively. Samples were pooled together based on purity into two fractions.

xiii. Total Purification of SaPGPase(HT) and SaPGPase

The purpose of introducing the His•Tag to the end of the protein was to simplify purification and increase the purity of the final enzyme. Figure 24 shows the overall purification of both SaPGPase(HT) and SaPGPase. Tables 7 and 8 show the details of the purification of each protein. As can be seen by comparing Figure 24A and Figure 24B, the addition of the His•Tag did increase the purity of the enzyme.

Table 7: Purification of *S. aureus* PGPase(HT)

Purification Step	**Volume** (mL)	**Protein Concentration** (mg/mL)	**Total Protein** (mg)
Sonicated Supe	7.0	24.3	170
Ni^{2+} Affinity	1.4	33.3	47
Size Exclusion	1.4	20.6	29

Table 8: Purification of *S. aureus* PGPase

Purification Step	**Volume** (mL)	**Protein Concentration** (mg/mL)	**Total Protein** (mg)
Freeze-Thaw Supe	8.0	5.8	46
80% Ammonium Sulfate	1.7	22.3	38
Size Exclusion Fraction A	1.7	11.5	19
Size Exclusion Fraction B	0.6	12.4	7

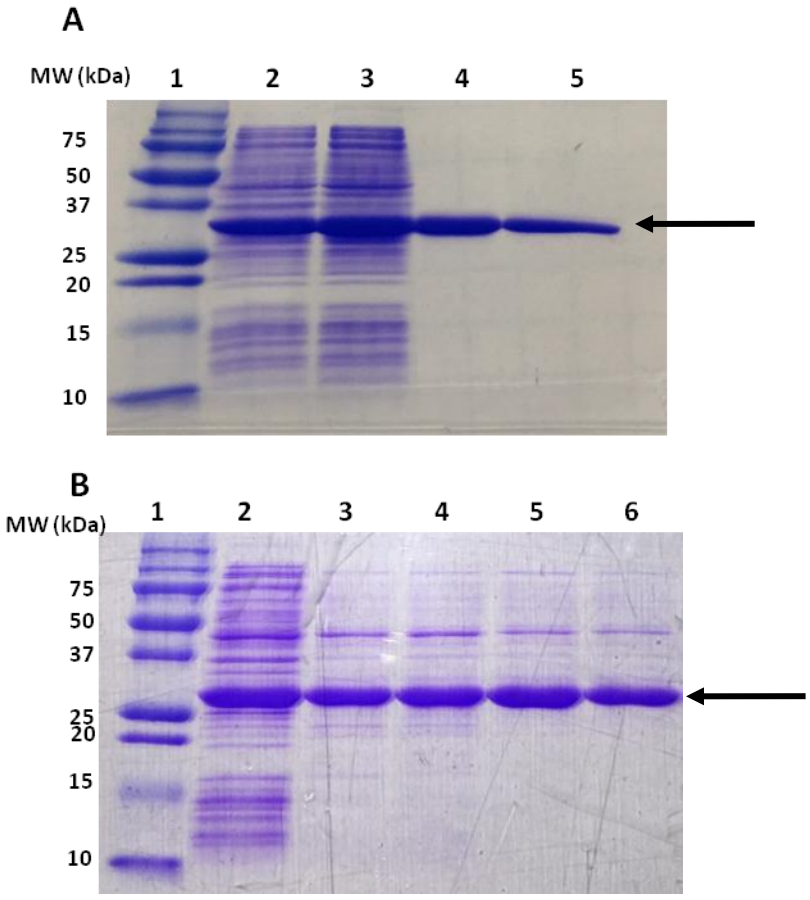

Figure 24: Purification of *S. aureus* PGPase(HT) and PGPase. **A:** SaPGPase(HT). Lane 1: MWMs, Lane 2: crude extract, Lane 3: sonicated supernatant, Lane 4: Ni-NTA purified, Lane 5: size exclusion purified. **B:** SaPGPase. Lane 1: MWMs, Lane 2: crude extract, Lane 3: pooled freeze-thaw extract, Lane 4: 80% ammonium sulfate pellet, Lane 5: size exclusion fraction A, Lane 6: 80% ammonium sulfate pellet, Fraction A.

xiv. Characterization of *S. aureus* phosphoglycolate phosphatase

For all characterization and kinetics, a unit of enzymatic activity is defined as 1 μmol of substrate cleaved per minute. *S. aureus* PGPase and PGPase(HT) were characterized to determine the best substrate, divalent metal ion, and pH needed to ensure optimal enzymatic activity. Experiments were carried out first with the relatively inexpensive, biologically non-natural, substrate-analog p-nitrophenyl phosphate to conserve the expensive and difficult to obtain substrate 2-phosphoglycolate, though most of the data is reported for the biologically significant 2-phosphoglycolate.

a. Substrate Specificity

For both the native and His•Tagged versions of the PGPase, the best substrate is 2-phosphoglycolate. The next best substrate is the non-natural substrate-analog p-nitrophenyl phosphate (Table 9**)**. No other substrate from our substrate library had more than 5% relative activity in comparison to 2-phosphoglycolate.

Table 9: Substrate specificity of SaPGPase

	SaPGPase(HT)		**SaPGPase**	
Substrate	**Specific Activity** (U/mg)[a]	**Relative Activity** (%)	**Specific Activity** (U/mg)[a]	**Relative Activity** (%)
2-phosphoglycolate	128.3	100	129.9	100
p-nitrophenyl phosphate	55.7	43	34.7	27
Phosphoenolpyruvate	6.2	5	4.8	4
fructose-1-phosphate	4.8	4	3.5	3
glucose-1,6-bisphosphate	4.7	4	1.1	1
2-phosphoglycerol	4.4	3	1.7	1
glyceraldehyde-3-phosphate	2.8	2	<1	<1
thiamine diphosphate	2.7	2	3.1	2
arabinose-5-phosphate	<1	<1	<1	<1
pyridoxal phosphate	<1	<1	<1	<1
3-phosphoglycerol	<1	<1	<1	<1

[a]: One unit of enzyme hydrolyses 1 μmol of substrate per min.

b. pH optimum

The pH optimum was determined using magnesium chloride as the metal ion cofactor and 2 phosphoglycolate as the substrate. Buffers of acetate (pH 4.0-5.5), MES•NaOH (pH 5.0-7.0), and glycine (pH 8.0-10.0) were used. As shown in Figure 25, the enzyme has optimal activity at pH 6.0.

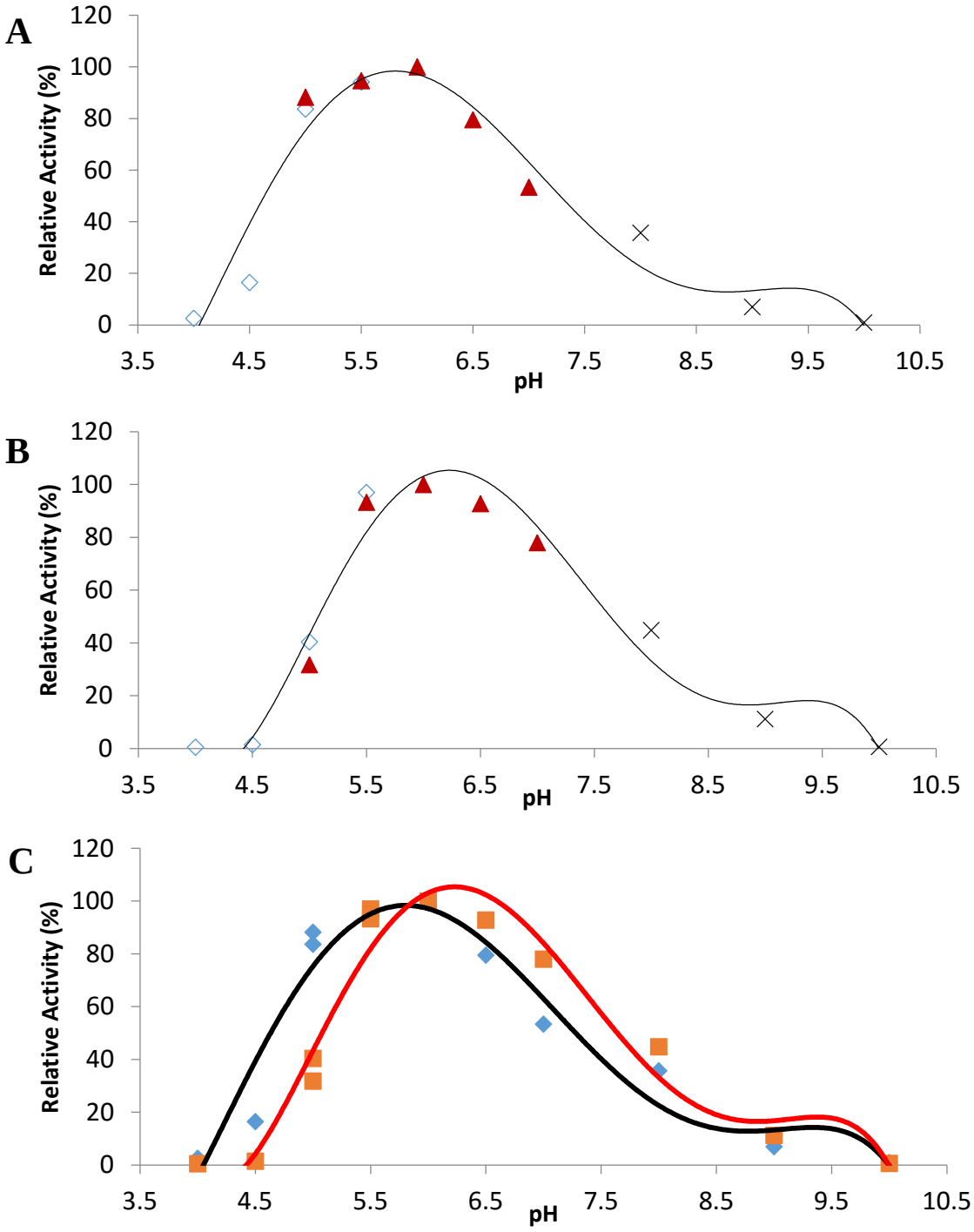

Figure 25: Effect of pH on PGPase activity. **A:** PGPase **B:** PGPase (HT). Reactions were carried out at 37 ˚C with 4 mM 2-phosphoglycolate, 10 mM Mg^{2+}, 1 mM DTT. and 50 mM acetate (◊), 50 mM MES•NaOH (▲) or 50 mM glycine (X) at various pH values. **C:** Overlay of the proteins with PGPase (◊, black line) and PGPase (HT) (■, red line).

c. Divalent metal ion requirements

S. aureus PGPase absolutely requires a divalent metal ion cofactor for activity. The best metal ion cofactor was determined for PGPase(HT) with solutions of Mg^{2+}, Mn^{2+}, Co^{2+}, Zn^{2+}, and Ca^{2+} ranging in concentration from 1-50 mM (Figure 26**)**. The metal ion yielding the highest activity was Mg^{2+} at a concentration of 10 mM. Mn^{2+} and Co^{2+} were the next best metals with ~20% relative activity, while Zn^{2+} and Ca^{2+} gave no activity.

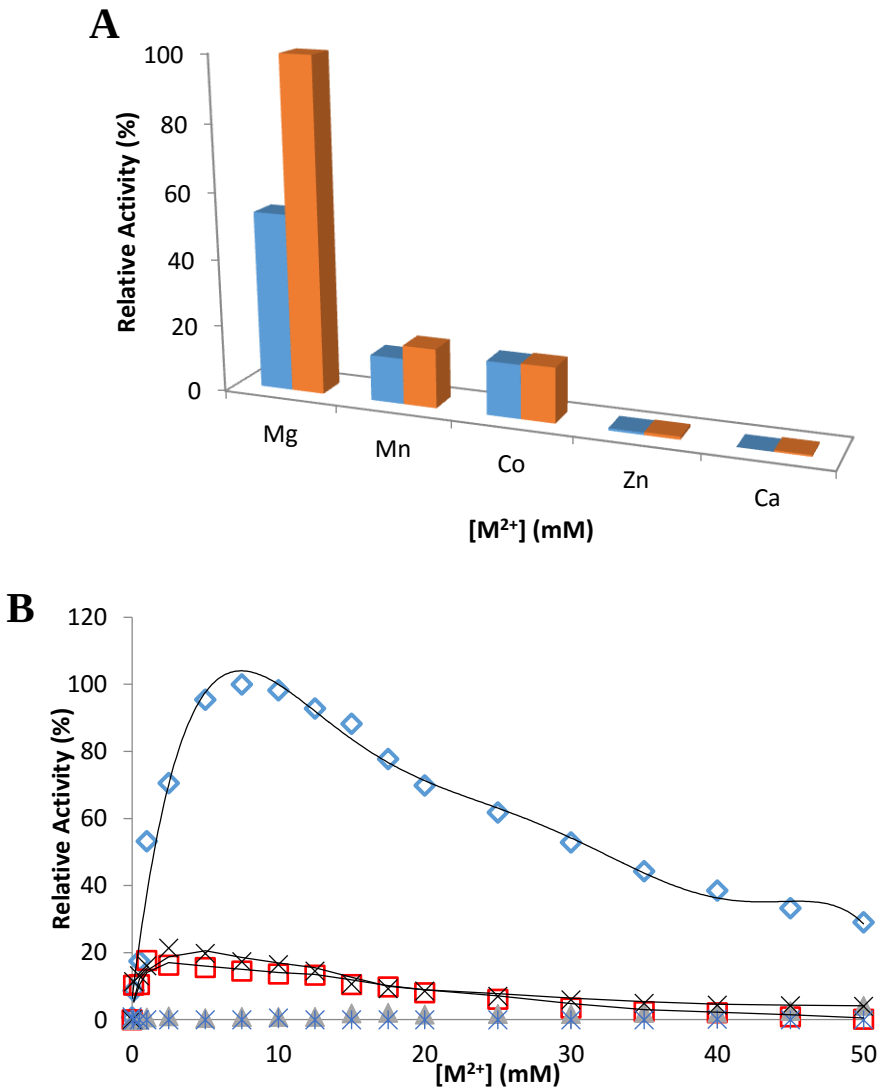

Figure 26: Effect of divalent metal ion concentration on PGPase(HT) activity. Reactions were carried out at 37 ˚C with 4 mM 2-phosphoglycolate, 50 mM MES•NaOH (pH 6.0), 1 mM DTT, 0.0021 µg PGPase(HT), and either **A:** 1 (blue) or 10 (orange) mM Mg^{2+}, Mn^{2+}, Co^{2+}, Zn^{2+}, or Ca^{2+} or **B:** various concentrations of Mg^{2+} (◊), Mn^{2+} (□), Co^{2+} (X), Zn^{2+} (▲), and Ca^{2+} (∗)**.** Mg^{2+} gave optimal activity while $Zn^{2+}$and Ca^{2+} gave no activity.

S. aureus PGPase enzyme was tested using either 1 or 10 mM of Mg^{2+}, Mn^{2+}, Co^{2+}, Zn^{2+}, and Ca^{2+}. Of these, 10 mM $Mg^{2+}$was shown to yield the highest activity, and a more complete range of Mg^{2+} concentrations was used from 1- 50 mM (Figure 27). As with the PGPase(HT), PGPase has optimal activity at 10 mM Mg^{2+}, with Mn^{2+} and Co^{2+}being the next best metals with ~40% relative activity and virtually no activity with either Zn^{2+} or Ca^{2+}.

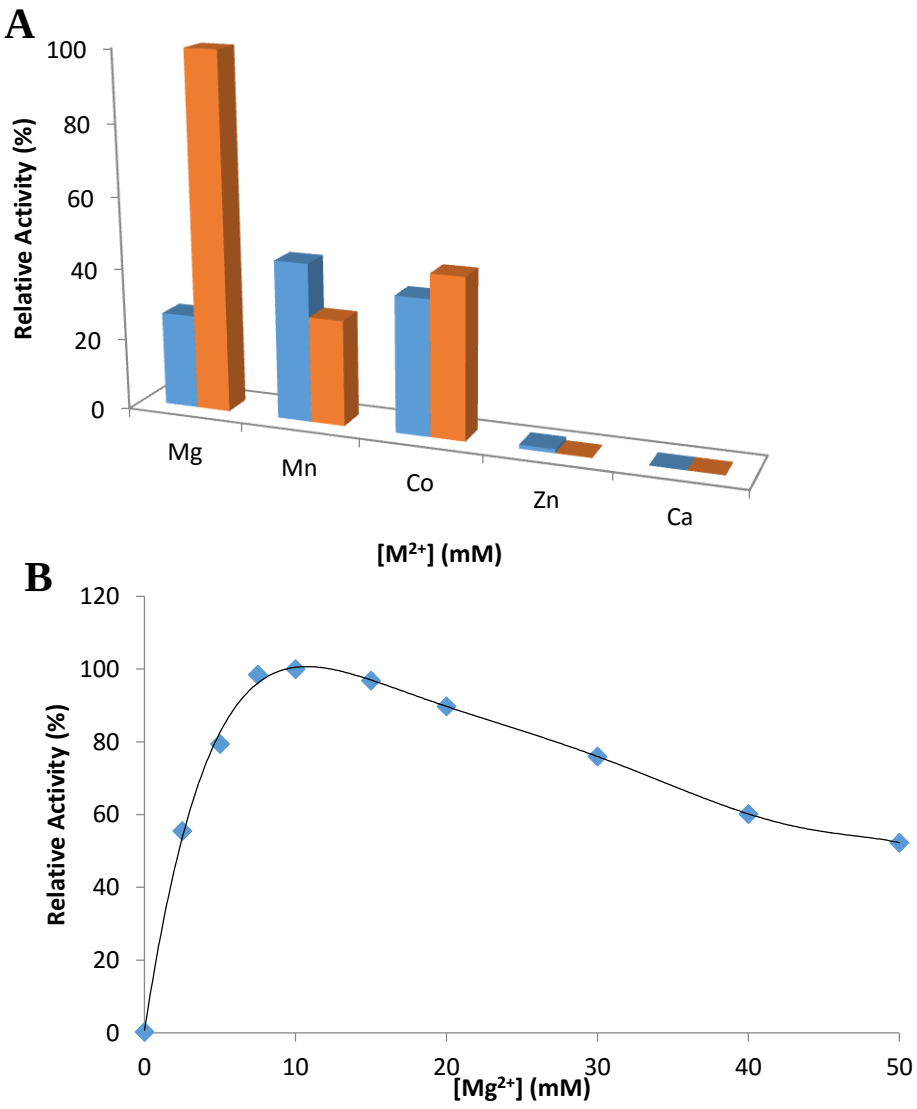

Figure 27: Effect of divalent metal ion concentration on PGPase activity. Reactions were carried out at 37 ˚C with 4 mM 2-phosphoglycolate, 50 mM MES•NaOH (pH 6.0), 1 mM DTT, 0.003µg PGPase, and either **A:** 1 (blue) or 10 (orange) mM Mg^{2+}, Mn^{2+}, Co^{2+}, Zn^{2+}, or Ca^{2+} or **B:** various concentrations of Mg^{2+}. Mg^{2+} gave optimal activity while $Zn^{2+}$and Ca^{2+} gave no activity.

d. Kinetic analysis of *S. aureus* PGPase(HT) and PGPase

Kinetic analysis was carried out for both forms of the enzyme to ensure that the addition of a His•Tag did not interfere with enzymatic activity. Two different concentrations of the enzyme were tested against varying concentrations of the substrate 2-phosphoglycolate for both native and tagged PGPase. An additional analysis was performed using PGPase(HT) and p-nitrophenyl phosphate. V_{max} and K_m values were determined from nonlinear regression graphs (Figures 28A, 29A, and 30A**)**. The graphs show that both forms of the enzyme follow Michaelis-Menten kinetics. The k_{cat} was calculated under the assumption that the enzyme is a monomer (as determined by size exclusion chromatography). The kinetic values (V_{max}, K_m, k_{cat}, and k_{cat}/K_m) are in Table 8. Comparison of the catalytic efficiencies (k_{cat}/K_m) of native and His•Tagged enzyme shows that the addition of the His•Tag did not impact the enzymatic activity with k_{cat}/K_m values of 163.5 ± 20.8 $mM^{-1} \cdot s^{-1}$ and 176.4 ± 35.3 $mM^{-1} \cdot s^{-1}$, respectively. It should be noted that the apparent difference in k_{cat} values is caused by different protein weights due to the additional His•Tag (27.9 kDa versus 29.3 kDa).

Table 10: Kinetic values for PGPase. For 2-phosphoglycolate (PG), the standard phosphatase assay was used with 0.1-20 mM substrate. For p-nitrophenyl phosphate (pNpp), the standard phosphatase assay was used with 0.1-40 mM substrate. V_{max} and K_m were determined from a nonlinear regression analysis and k_{cat} was calculated from V_{max} assuming that PGPase is a monomer with a molecular mass of either 27.8 kDa (untagged) or 29.3 kDa (His•Tagged).

Enzyme	Substrate	V_{max} (U/mg)	k_{cat} (s^{-1})	K_m (mM)	k_{cat}/K_m ($mM^{-1} \cdot s^{-1}$)
PGPase	PG	822.4 ± 27.0	382.4 ± 12.6	2.34 ± 0.22	163.5 ± 20.8
PGPase (HT)	PG	969.1 ± 51.8	556.8 ± 29.8	3.16 ± 0.47	176.4 ± 35.3
PGPase (HT)	pNpp	117.4 ± 2.7	67.5 ± 1.6	6.54 ± 0.45	10.3 ± 1.0

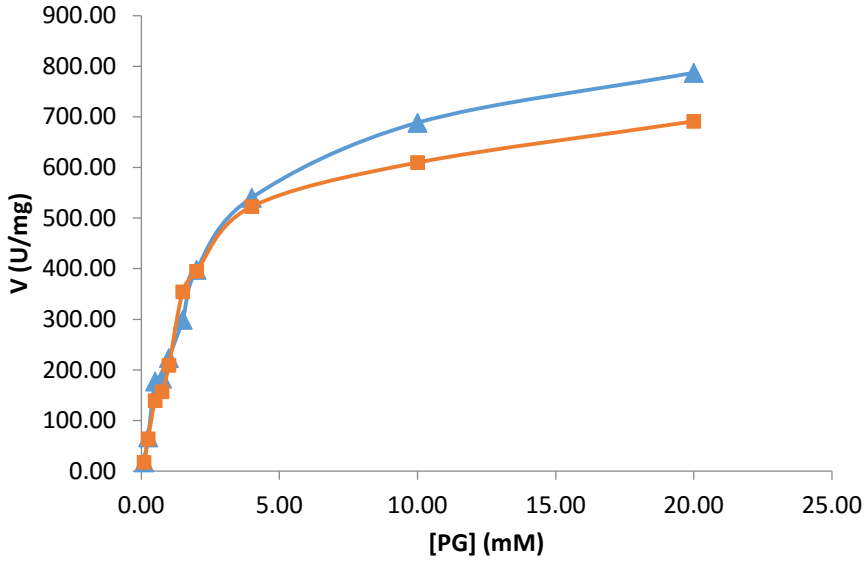

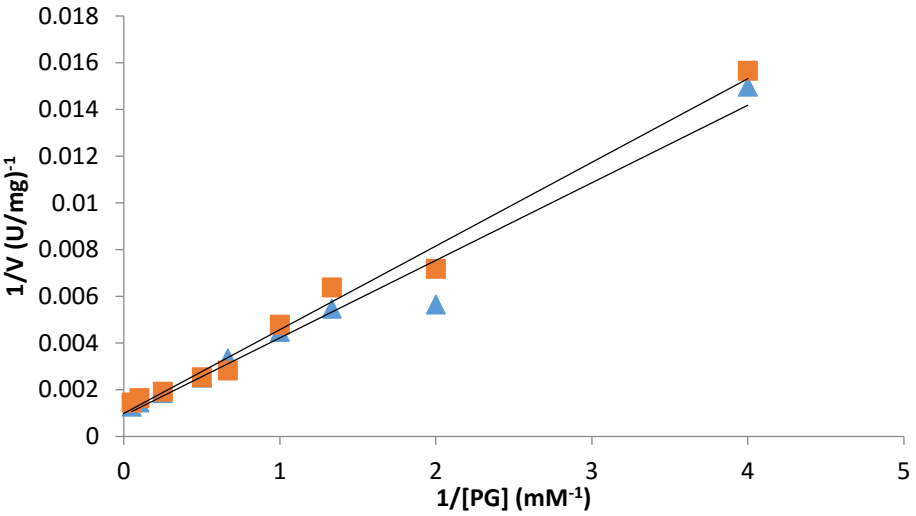

Figure 28: Nonlinear regression and Lineweaver-Burke plot for *S. aureus* PGPase with 2-phosphoglycolate. 0.1-20 mM 2-PG with either 0.57 ng PGPase (▲) or 0.29 ng PGPase (■).

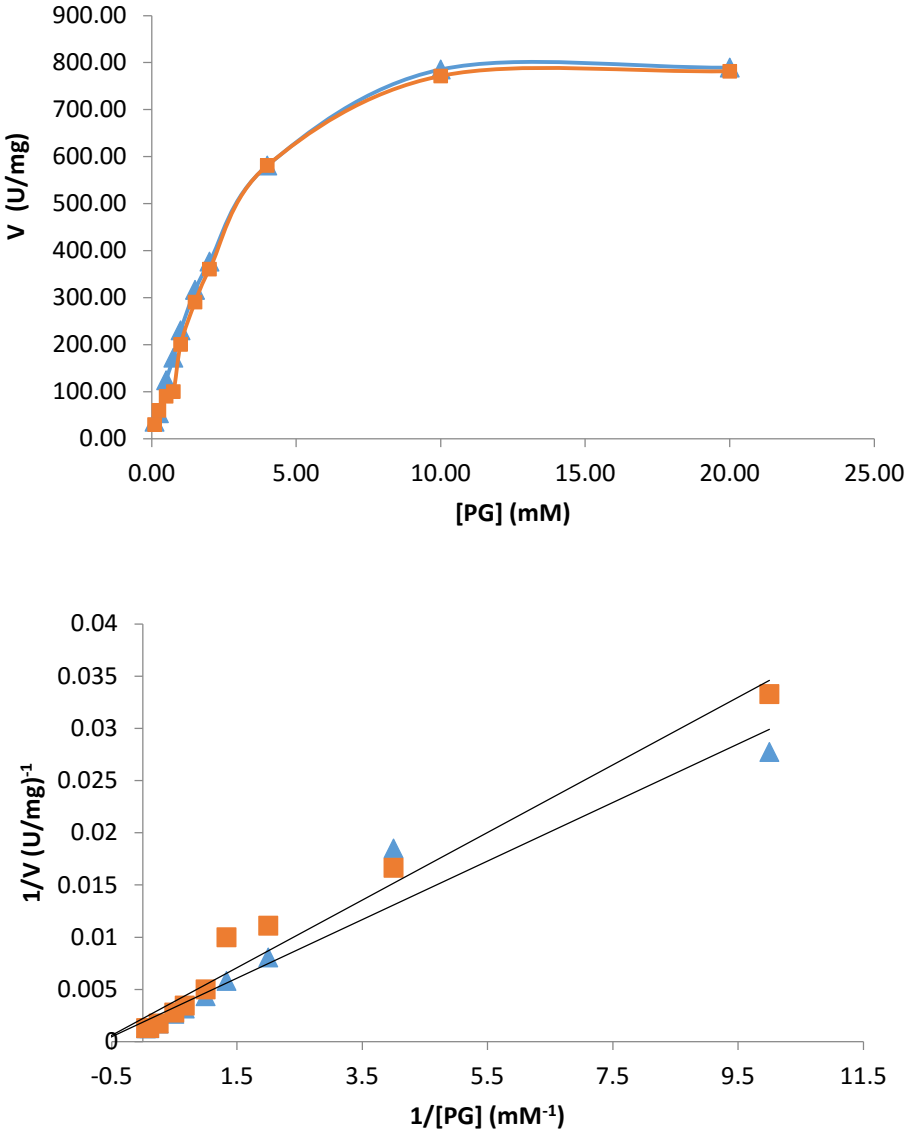

Figure 29: Nonlinear regression and Lineweaver-Burke plot for *S. aureus* PGPase(HT) with 2-phosphoglycolate . 0.1-20 mM 2-PG 0.83 ng PGPase (HT) (▲) or 0.17 ng PGPase(HT) (■).

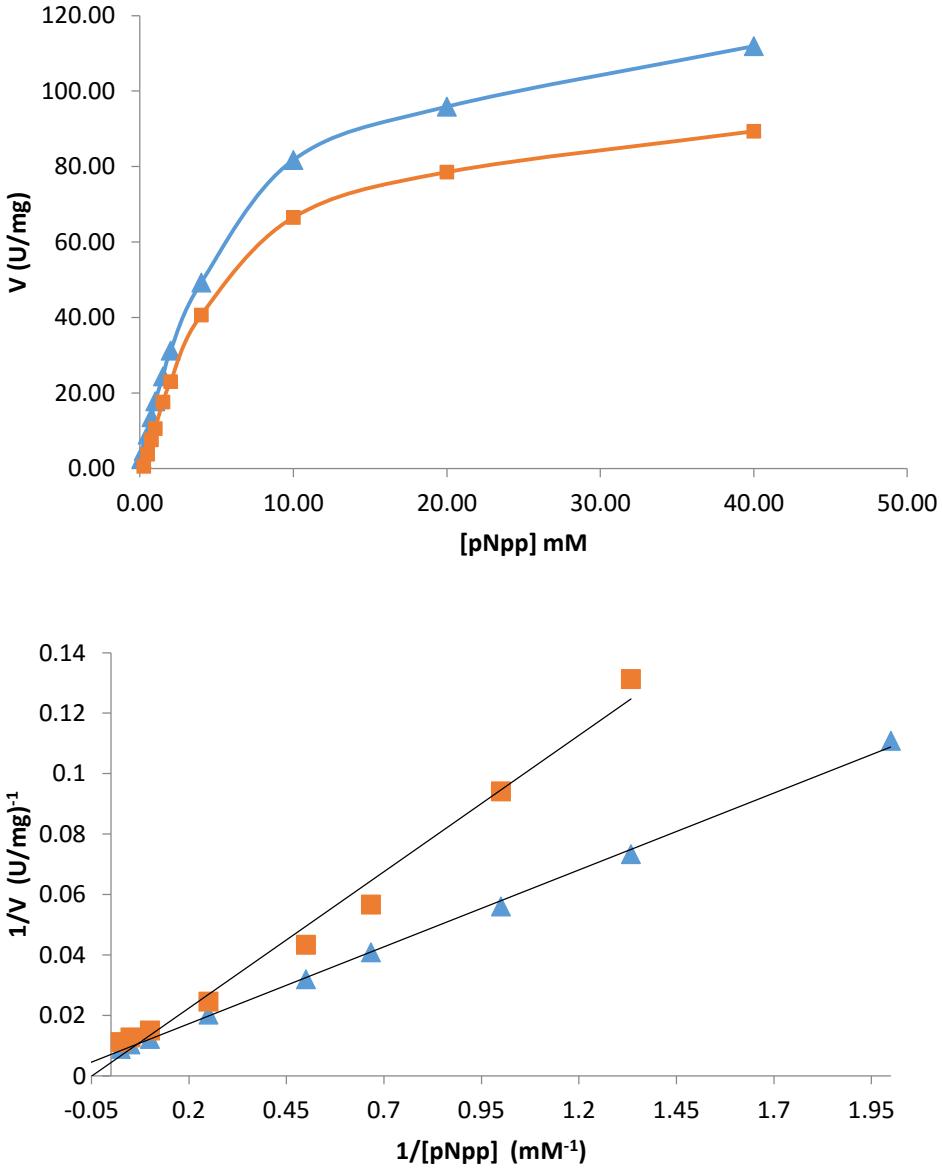

Figure 30: Nonlinear regression and Lineweaver-Burke plot for *S. aureus* PGPase(HT) with p-nitrophenyl phosphate. 0.1-40 mM pNpp with either 17 ng PGPase(HT) (▲) or 8 ng PGPase(HT) (■).

IV. Conclusions

Our lab has been systematically characterizing members of the pNppase subfamily of the HAD superfamily. When Begun et al. reported a subfamily member from *S. aureus* that acted as a virulence factor; we decided to characterize it next. The authors of the study identified the protein as an ortholog of the NagD UMPase from *E. coli* due to similar amino acid sequence alignment. However, we suspected this protein was not an UMPase, as it was no closer in sequence to NagD than to the other subfamily members. The enzymatic activity of this protein was not known prior to the work done for this thesis.

The *S. aureus* SAV0929 synthetic gene was designed and subcloned into pET11b and pET19b plasmids for overexpression; subcloning into the pET19b plasmid incorporated a His•Tag at the N-terminal end of the protein. Both forms of the protein (tagged and untagged) have been expressed, determined to be soluble, purified, and characterized. Purification of the native protein involved freeze-thaw cycles followed by concentration via ammonium sulfate. Purification of His•Tagged protein involved sonication followed by Ni-NTA affinity chromatography and concentration via centrifugal filtration. Both proteins were further purified by size exclusion chromatography.

Enzyme assays have been done, for both forms of the protein, to determine substrate specificity (2-phosphoglycolate is the best substrate), pH optimum (pH 6.0), and divalent metal ion optimum (10 mM Mg^{2+}). Kinetic values were determined with no significant difference observed between the two forms of the protein. That, along with the same results for substrate specificity, pH optimum, and divalent metal ion requirements indicates that the His•Tag does not interfere with enzymatic activity. However, the His•Tag enabled us to purify the protein more easily.

We determined that the protein encoded by SAV0929 is a phosphoglycolate phosphatase and not an UMPase like NagD. Thus showing that assigning function based on sequence similarity is not always reliable and often the only way to determine function is to do the *in vitro* experiments.

The study by Begun et al. demonstrated that the enzyme is a virulence factor, but exactly how it confers virulence is not currently known. The phosphoglycolate phosphatase could be present to degrade 2-phosphoglycolate created from the repair of oxidatively damaged DNA. This would ensure the glycolytic enzyme triose phosphate isomerase is not inhibited, thus allowing TPI to function normally in glycolysis as well as moonlighting as an adhesion factor.

Future work will involve phenotypic and complementation studies furthering the virulence work by Begun et al.; however, that will require a collaboration with that research group. To determine the protein's structure, purified PGPase(HT) has been given to Dr. Roger Rowlett at Colgate University for x-ray crystallography. The crystal structure will be immensely useful in drug design if this enzyme is determined to be a reliable target for new antibiotics to combat drug resistant strains of *S. aureus.*

V. References

(1) Lewis, C. A., and Wolfenden, R. (2008) Uroporphyrinogen decarboxylation as a benchmark for the catalytic proficiency of enzymes. *Proc. Natl. Acad. Sci.* **105**, 17328–17333.

(2) Copeland, R. (2000) A brief history of enzymology, in *Enzymes: A practical introduction to structure, mechanism, and data analysis* 2nd ed., pp 1–10. John & Wiley Sons Inc, New York.

(3) Mills, C. L., Beuning, P. J., and Ondrechen, M. J. (2015) Biochemical functional predictions for protein structures of unknown or uncertain function. *Comput. Struct. Biotechnol. J.* **13**, 182–191.

(4) Gerlt, J. A., Allen, K. N., Almo, S. C., Armstrong, R. N., Patricia, C., Cronan, J. E., Dunaway-mariano, D., Imker, H. J., Matthew, P., Minor, W., Poulter, C. D., Raushel, F. M., Sali, A., and Brian, K. (2011) The Enzyme Function Initiative. *Biochemistry* **50**, 9950–9962.

(5) Burroughs, A. M., Allen, K. N., Dunaway-Mariano, D., and Aravind, L. (2006) Evolutionary genomics of the HAD superfamily: understanding the structural adaptations and catalytic diversity in a superfamily of phosphoesterases and allied enzymes. *J. Mol. Biol.* **361**, 1003–34.

(6) Seifried, A., Schultz, J., and Gohla, A. (2013) Human HAD phosphatases: structure, mechanism, and roles in health and disease. *FEBS J.* **280**, 549–71.

(7) Koonin, E. V, and Tatusov, R. L. (1994) Computer analysis of bacterial haloacid dehalogenases defines a large superfamily of hydrolases with diverse specificity. Application of an iterative approach to database search. *J. Mol. Biol.* **244**, 125–132.

(8) Tremblay, L. W., Dunaway-mariano, D., and Allen, K. N. (2006) Structure and activity analyses of *Escherichia coli* K-12 NagD provide insight into the evolution of biochemical function in the haloalkanoic acid dehalogenase. *Biochemistry.***45**, 1183–1193.

(9) Kuznetsova, E., Proudfoot, M., Gonzalez, C. F., Brown, G., Omelchenko, M. V, Borozan, I., Carmel, L., Wolf, Y. I., Mori, H., Savchenko, A. V, Arrowsmith, C. H., Koonin, E. V, Edwards, A. M., and Yakunin, A. F. (2006) Genome-wide analysis of substrate specificities of the *Escherichia coli* haloacid dehalogenase-like phosphatase family. *J. Biol. Chem.* **281**, 36149–61.

(10) Allen, K. N., and Dunaway-Mariano, D. (2004) Phosphoryl group transfer: evolution of a catalytic scaffold. *Trends Biochem. Sci.* **29**, 495–503.

(11) Lu, Z., Dunaway-Mariano, D., and Allen, K. N. (2008) The catalytic scaffold of the haloalkanoic acid dehalogenase enzyme superfamily acts as a mold for the trigonal bipyramidal transition state. *Proc. Natl. Acad. Sci. U. S. A.* **105**, 5687–92.

(12) Tirrell, I. M., Wall, J. L., Daley, C. J., Denial, S. J., Tennis, F. G., Galens, K. G., and O'Handley, S. F. (2006) YZGD from *Paenibacillus thiaminolyticus*, a pyridoxal phosphatase of the HAD (haloacid dehalogenase) superfamily and a versatile member of the Nudix (nucleoside diphosphate x) hydrolase superfamily. *Biochem. J.* **394**, 665–74.

(13) Fondas, M. L. (1992) Purification and characterization of vitamin B_6-phosphate phosphatase from human erythrocytes. *J. Biol. Chem.* **267**, 15978–15983.

(14) Reaves, M. L., Young, B. D., Hosios, A. M., Xu, Y.-F., and Rabinowitz, J. D. (2013) Pyrimidine homeostasis is accomplished by directed overflow metabolism. *Nature* **500**, 237–241.

(15) Godinho, L. M., and de Sá-Nogueira, I. (2011) Characterization and regulation of a bacterial sugar phosphatase of the haloalkanoate dehalogenase superfamily, AraL, from *Bacillus subtilis*. *FEBS J.* **278**, 2511–24.

(16) Mamedov, T. G., Suzuki, K., Miura, K., Kucho Ki, K., and Fukuzawa, H. (2001) Characteristics and sequence of phosphoglycolate phosphatase from a eukaryotic green alga *Chlamydomonas reinhardtii*. *J. Biol. Chem.* **276,** 45573–9.

(17) Pellicer, M. T., Nun, M. F., Aguilar, J., Badia, J., and Baldoma, L. (2003) Role of 2-phosphoglycolate phosphatase of *Escherichia coli* in metabolism of the 2-Phosphoglycolate formed in DNA repair. *J. Bacter.* **185**, 5815–5821.

(18) Berg, J. M., Tymoczko, J. L., and Stryer, L. (2007) The Calvin Cycle, in *Biochemistry* (Moran, S., Ahr, K., and Baker, A., Eds.) 6th ed., pp 566–568. Teney, Sara, New York.

(19) Lolis, E., and Petsko, G. A. (1990) Crystallographic analysis of the complex between triosephosphate isomerase and 2-phosphoglycolate at 2.5-A resolution: implications for catalysis. *Biochemistry* **29**, 6619–6625.

(20) Mukherjee, S., Roychowdhury, A., Dutta, D., and Das, A. K. (2012) Crystal structures of triosephosphate isomerase from methicillin resistant *Staphylococcus aureus* MRSA252 provide structural insights into novel modes of ligand binding and unique conformations of catalytic loop. *Biochimie* **94,** 2532–2544.

(21) Bamba, T., Hasunuma, T., and Kondo, A. (2016) Disruption of PHO13 improves ethanol production via the xylose isomerase pathway. *AMB Express* **6**, 4.

(22) Van Vleet, J. H., Jeffries, T. W., and Olsson, L. (2008) Deleting the para-nitrophenyl phosphatase (pNppase), PHO13, in recombinant *Saccharomyces cerevisiae* improves growth and ethanol production on D-xylose. *Metab. Eng.* **10**, 360–369.

(23) Ni, H., Laplaza, J. M., and Jeffries, T. W. (2007) Transposon mutagenesis to improve the growth of recombinant *Saccharomyces cerevisiae* on D-xylose. *Appl. Environ. Microbiol.* **73**, 2061–2066.

(24) Mosier, N., Wyman, C., Dale, B., Elander, R., Lee, Y. Y., Holtzapple, M., and Ladisch, M. (2005) Features of promising technologies for pretreatment of lignocellulosic biomass. *Bioresour. Technol.* **96**, 673–686.

(25) Rose, Z. B., Dube, S., and Chem, J. B. (1978) Phosphoglycerate mutase. Kinetics and effects of salts on the mutase and bisphosphoglycerate phosphatase activities of the enzyme from chicken breast muscle . *J. Biol. Chem.* **253**, 8583–8592.

(26) Sasaki, H., Fujii, S., Yoshizaki, Y., Nakashima, K., and Kaneko, T. (1987) Phosphoglycolate synthesis by human erythrocyte pyruvate kinase. *Acta Haematol.* **77**, 83–6.

(27) Kuroda, M., Ohta, T., Uchiyama, I., Baba, T., Yuzawa, H., Kobayashi, I., Cui, L., Oguchi, A., Aoki, K., Nagai, Y., Lian, J., Ito, T., Kanamori, M., Matsumaru, H., Maruyama, A., Murakami, H., Hosoyama, A., Mizutani-Ui, Y., Takahashi, N. K., Sawano, T., Inoue, R., Kaito, C., Sekimizu, K., Hirakawa, H., Kuhara, S., Goto, S., Yabuzaki, J., Kanehisa, M., Yamashita, A., Oshima, K., Furuya, K., Yoshino, C., Shiba, T., Hattori, M., Ogasawara, N., Hayashi, H., and Hiramatsu, K. (2001) Whole genome sequencing of meticillin-resistant *Staphylococcus aureu*s. *Lancet* **357**, 1225–1240.

(28) Orenstein, A. (1998) The discovery and naming of *Staphylococcus aureus*. *Infect. Dis. Antimicrob. agents* 1880–1881. http://www.antimicrobe.org/h04c.files/history/S-aureus.pdf (accessed May 2016)

(29) Newsom, S. W. B. (2008) Ogston's coccus. *J. Hosp. Infect.* **70**, 369–372.

(30) Lindsay, J. a, and Holden, M. T. G. (2006) Understanding the rise of the superbug: investigation of the evolution and genomic variation of *Staphylococcus aureus*. *Funct. Integr. Genomics* **6**, 186–201.

(31) Patel, H., Vaghasiya, Y., Vyas, B. R. M., and Chanda, S. (2012) Antibiotic-resistant *Staphylococcus aureus*: A challenge to researchers and clinicians. *Bacteriol. J.* **2**, 23–45.

(32) Crossley, K. B., Jefferson, K., Archer, G. L., and Fowler, V. (2009) Staphylococci in Human Disease (Crossley, K. B., Jefferson, K. K., Archer, G. L., and Fowler, V. G., Eds.). Wiley-Blackwell, Oxford, UK.

(33) Rajamuthiah, R., Fuchs, B. B., Jayamani, E., Kim, Y., Larkins-Ford, J., Conery, A., Ausubel, F. M., and Mylonakis, E. (2014) Whole animal automated platform for drug discovery against multi-drug resistant *Staphylococcus aureus*. *PLoS One* **9**, e89189.

(34) Otto, M. (2009) Understanding the epidemic of community-associated MRSA and finding a cure: are we asking the right questions? *Expert Rev Anti Infect Ther* **7**, 141–143.

(35) Lindsay, J. A. (2010) Genomic variation and evolution of *Staphylococcus aureus*. *Int. J. Med. Microbiol.* **300**, 98–103.

(36) Chambers, H. F., and Deleo, F. R. (2009) Waves of resistance: *Staphylococcus aureus* in the antibiotic era. *Nat Rev Microbiol* **7,** 629–641.

(37) Feng, Y., Chen, C. J., Su, L. H., Hu, S., Yu, J., and Chiu, C. H. (2008) Evolution and pathogenesis of *Staphylococcus aureus*: Lessons learned from genotyping and comparative genomics. *FEMS Microbiol. Rev.* **32**, 23–37.

(38) Boneca, I. G., and Chiosis, G. (2003) Vancomycin resistance: occurrence, mechanisms and strategies to combat it. *Expert Opin. Ther. Targets* **7**, 311–328.

(39) Begun, J., Sifri, C. D., Goldman, S., Calderwood, S. B., and Ausubel, F. M. (2005) *Staphylococcus aureus* virulence factors identified by using a high-throughput *Caenorhabditis elegans*-killing model. *Infect. Immun.* **73**, 872–7.

(40) Henderson, B., and Martin, A. (2011) Bacterial virulence in the moonlight: multitasking bacterial moonlighting proteins are virulence determinants in infectious disease. *Infect. Immun.* **79,** 3476–91.

(41) Pancholi, V., and Chhatwal, G. S. (2003) Housekeeping enzymes as virulence factors for pathogens. *Int. J. Med. Microbiol.* **293**, 391–401.

(42) Furuya, H., and Ikeda, R. (2009) Interaction of triosephosphate isomerase from the cell surface of *Staphylococcus aureus* and alpha-(1->3)-mannooligosaccharides derived from glucuronoxylomannan of *Cryptococcus neoformans*. *Microbiology* **155**, 2707–13.

(43) Pancholi, V., and Fischetti, V. A. (1997) A novel plasminogen/plasmin binding protein on the surface of group A streptococci. *Adv. Exp. Med. Biol.* **418**, 597–9.

(44) Ikeda, R., Saito, F., Matsuo, M., Kurokawa, K., Sekimizu, K., Yamaguchi, M., and Kawamoto, S. (2007) Contribution of the mannan backbone of cryptococcal glucuronoxylomannan and a glycolytic enzyme of *Staphylococcus aureus* to contact-mediated killing of *Cryptococcus neoformans*. *J. Bacteriol.* **189**, 4815–26.

(45) Yamaguchi, M., Ikeda, R., Nishimura, M., and Kawamoto, S. (2010) Localization by scanning immunoelectron microscopy of triosephosphate isomerase, the molecules responsible for contact-mediated killing of Cryptococcus, on the surface of *Staphylococcus*. *Microbiol. Immunol.* **54**, 368–70.

(46) Novagen. (2003) pET System Manual. *Biosystems* 1–68. http://richsingiser.com/4402/NovagenpETsystemmanual.pdf (accessed April 17, 2016)

(47) Valenti, L. E., De Pauli, C. P., and Giacomelli, C. E. (2006) The binding of Ni(II) ions to hexahistidine as a model system of the interaction between nickel and His-tagged proteins. *J. Inorg. Biochem.* **100**, 192–200.

(48) Skoog, D. A., Holler, F. J., and Crouch, S. R. (2007) Size Exclusion Chromatography, in *Principles of Instrumental Analysis* (Kiselica, S., Broyer, R., Ed.)6th ed., pp 844-848, David Harris, Belmont, California.

(49) Ames, B. N., and Dubin, D. T. (1960) The role of polyamines in the neutralization of bacteriophage deoxyribonucleic acid. *J. Biol. Chem.* **235**, 769–775.

(50) Sambrok, J., Fritsch, E. F., Maniatis, T. (1989) Ligation reactions, in *Molecular cloning: a laboratory manual* 2nd ed., pp 1.63-1.67. Cold Spring Harbor Laboratory Press, Plainview, NY.

VI. Acknowledgments

I would like to thank the members of Dr. O'Handley's research lab, of which there are many, for their support in the lab and for providing a pleasant environment that greatly increased productivity. I would specifically like to thank fellow graduate students Courtney Kellogg and Peipei Zhu for their guidance on procedures and experiments as well as engaging in intellectual conversations.

I am most grateful for all the time and energy Dr. O'Handley has put into training me to be a good scientist. Her guidance and encouragement on this project as well as a great mentor has been invaluable. I would like to thank the members of my committee (Dr. Austin Gehret, Dr. André Hudson, and Dr. Lea Michel) for their support and feedback throughout this project.

I wish to thank the RIT School of Chemistry and Materials Science for the opportunity to conduct this research as well as gain experience in teaching. I would like to thank the Office of Graduate Studies for their Graduate Research and Creativity Grant that helped fund this project.

Finally, I wish to thank my wife, without whom I do not think I would have had the endurance to finish.

VII. Appendix

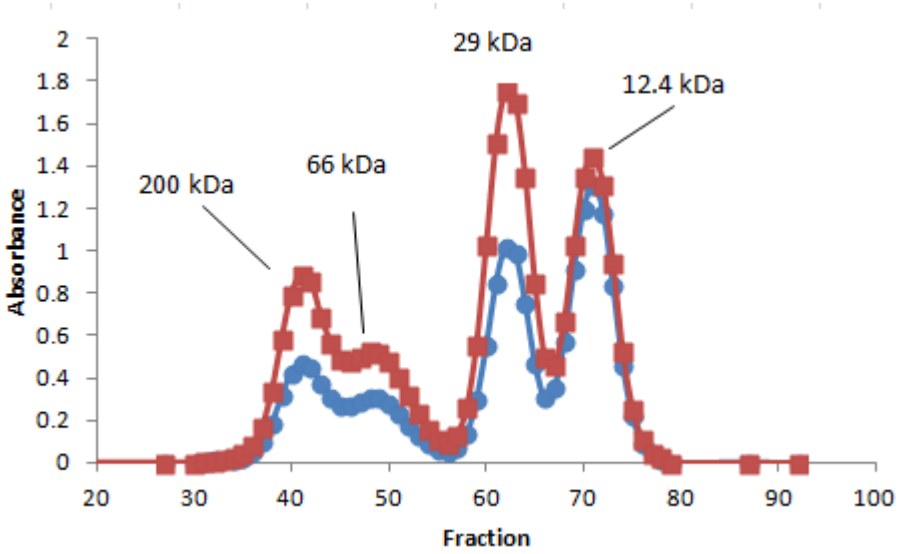

Figure 31: Size exclusion chromatography of protein standards.
Absorbance (● A_{260}, ■ A_{280}) vs. fraction. 200 kDa (β-amylase), 66 kDa (BSA), 29 kDa (carbonic anhydrase) and 12.4 kDa (cytochrome C) peaks are indicated.

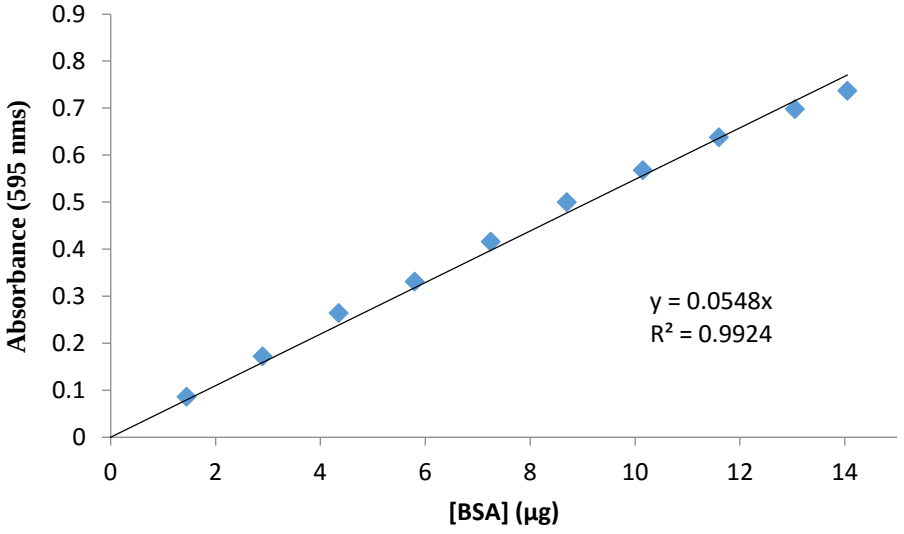

Figure 32: Standard curve for Bradford protein analysis. Using BSA standard.